

ORIGINAL ARTICLE

USP51/PD-L1/ITGB1-deployed juxtacrine interaction plays a cell-intrinsic role in promoting chemoresistant phenotypes in non-small cell lung cancer

Jianjun Li^{1,2} | Xuechun Xiao¹ | Yang Ou¹ | Lixia Cao¹ | Min Guo¹ |
 Chunchun Qi¹ | Zhaoyang Wang¹ | Yuxin Liu¹ | Qiuying Shuai¹ | Hang Wang¹ |
 Peiqing Sun³ | Yi Shi¹ | Guang Yang⁴ | Shuang Yang^{1,5} 

¹Tianjin Key Laboratory of Tumor Microenvironment and Neurovascular Regulation, School of Medicine, Nankai University, Tianjin, P. R. China

²Department of Pulmonary and Critical Care Medicine, The First Affiliated Hospital of Soochow University, Suzhou, Jiangsu, P. R. China

³Department of Cancer Biology, Wake Forest University School of Medicine, Winston-Salem, NC, USA

⁴College of Pharmacy, Nankai University, Tianjin, P. R. China

⁵Institute of Transplantation Medicine, Nankai University, Tianjin, P. R. China

Correspondence

Shuang Yang, School of Medicine, Nankai University, Tianjin 300071, P. R. China.

Email: yangshuang@nankai.edu.cn

Guang Yang, College of Pharmacy, Nankai University, Tianjin 300071, P. R. China.

Email: guang.yang@nankai.edu.cn

Funding information

International Science and Technology

Cooperation Project of China,

Grant/Award Number: 2022YFE0133300;

National Natural Science Foundation of

China, Grant/Award Numbers: 82172801,

81972454

Abstract

Background: Programmed death ligand 1 (PD-L1) has been demonstrated to facilitate tumor progression and therapeutic resistance in an immune-independent manner. Nevertheless, the function and underlying signaling network(s) of cancer cell-intrinsic PD-L1 action remain largely unknown. Herein, we sought to better understand how ubiquitin-specific peptidase 51 (USP51)/PD-L1/integrin beta-1 (ITGB1) signaling performs a cell-intrinsic role in mediating chemotherapeutic resistance in non-small cell lung cancer (NSCLC). **Methods:** Western blotting and flow cytometry were employed for PD-L1 detection in NSCLC cell lines. Coimmunoprecipitation and pulldown analyses, protein deubiquitination assay, tissue microarray, bioinformatic analysis and molecular biology methods were then used to determine the significance

Abbreviations: AKT, AKT serine/threonine kinase; BIRC5, baculoviral IAP repeat containing 5; BRCA1, breast cancer gene 1; BRCA2, breast cancer gene 2; Co-IP, coimmunoprecipitation; CHX, Cycloheximide; DAPI, 4',6-diamidino-2-phenylindole; DDP, cisplatin; DHM, dihydromyricetin; DMEM, Dulbecco's Modified Eagle Medium; DMSO, dimethylsulfoxide; DTT, dithiothreitol; EGFR, epidermal growth factor receptor; ERK, extracellular regulated MAP kinase; FBS, fetal bovine serum; GAPDH, glyceraldehyde-3-phosphate dehydrogenase; GSS, glutathione synthetase; GST, glutathione S-transferase; HIF1 α , hypoxia inducible factor 1 alpha; JAK, Janus kinase; IFN- γ , interferon gamma; IRF1, interferon regulatory factor 1; ITGB1, integrin beta 1; LC, Lung cancer; MBP, maltose binding protein; MEK, MAP kinase-ERK kinase; mTOR, mechanistic target of rapamycin kinase; NEAA, non-essential amino acids; NF- κ B, nuclear factor-kappa B; NSCLC, non-small cell lung cancer; PD-L1, programmed death ligand 1; PI3K, phosphatidylinositol 3-kinase; RIPA, radio immunoprecipitation assay; shRNAs, short hairpin RNAs; SLC31A2, solute carrier family 31 member 2; SPOP, speckle type BTB/POZ protein; SPR, surface plasmon resonance; STAT1, signal transducer and activator of transcription 1; RNF31, ring finger protein 31; TRIM21, tripartite motif containing 21; TNF- α , tumor necrosis factor alpha; TNM, tumor node metastasis; Ub-AMC, C-terminal conjugate of ubiquitin with 7-amino-4-methylcoumarin; UCHL1, ubiquitin C-terminal hydrolase L1; USP7, ubiquitin specific peptidase 7; USP51, ubiquitin-specific peptidase 51; β -TrCP, beta-transducin repeat containing E3 ubiquitin protein ligase; γ H2AX, phosphorylated histone H2AX.

This is an open access article under the terms of the [Creative Commons Attribution-NonCommercial-NoDerivs](https://creativecommons.org/licenses/by-nc-nd/4.0/) License, which permits use and distribution in any medium, provided the original work is properly cited, the use is non-commercial and no modifications or adaptations are made.

© 2023 The Authors. *Cancer Communications* published by John Wiley & Sons Australia, Ltd. on behalf of Sun Yat-sen University Cancer Center.

of PD-L1 in NSCLC chemoresistance and associated signaling pathways in several different cell lines, mouse models and patient tissue samples. Ubiquitin-7-amido-4-methylcoumarin (Ub-AMC)-based deubiquitinase activity, cellular thermal shift and surface plasmon resonance (SPR) analyses were performed to investigate the activity of USP51 inhibitors.

Results: We provided evidence that cancer cell-intrinsic PD-L1 conferred the development of chemoresistance by directly binding to its membrane-bound receptor ITGB1 in NSCLC. At the molecular level, PD-L1/ITGB1 interaction subsequently activated the nuclear factor-kappa B (NF- κ B) axis to elicit poor response to chemotherapy. We further determined USP51 as a bona fide deubiquitinase that targeted the deubiquitination and stabilization of the PD-L1 protein in chemoresistant NSCLC cells. Clinically, we found a significant direct relationship between the USP51, PD-L1 and ITGB1 contents in NSCLC patients with chemoresistant potency. The elevated USP51, PD-L1 and ITGB1 levels were strongly associated with worse patient prognosis. Of note, we identified that a flavonoid compound dihydromyricetin (DHM) acted as a potential USP51 inhibitor and rendered NSCLC cells more sensitive to chemotherapy by targeting USP51-dependent PD-L1 ubiquitination and degradation in vitro and in vivo.

Conclusions: Together, our results demonstrated that the USP51/PD-L1/ITGB1 network potentially contributes to the malignant progression and therapeutic resistance in NSCLC. This knowledge is beneficial to the future design of advanced cancer therapy.

KEYWORDS

chemosensitivity, dihydromyricetin, immune-independence, ITGB1, non-small cell lung cancer, PD-L1, USP51

1 | BACKGROUND

Lung cancer (LC) contributes to the largest proportion of global cancer-associated mortality [1]. Non-small cell lung cancer (NSCLC) is the most prevalent form of LC, and makes up almost 85% of all LC cases [2]. Patients suffering from locally advanced or metastatic NSCLC typically obtain platinum-based chemotherapy [3]. Despite a consistent rate of initial responses, LC has relatively poor prognosis owing to drug resistance and tumor recurrence [4]. Therefore, it is urgent and necessary to elucidate the underlying mechanism of action behind chemoresistance in NSCLC in order to develop new and efficacious treatment for NSCLC.

Programmed death ligand 1 (PD-L1), otherwise named B7-H1 and CD274, is a 40 kDa transmembrane protein found on immune cells and multiple cancer cells, such as NSCLC [5, 6]. Recent studies have reported that PD-L1, an immune checkpoint protein, negatively modulates anticancer immunity via association with the

programmed cell death protein 1 (PD-1) receptor [7]. Despite multiple investigations examining the pivotal role of PD-L1 to inhibit T-cell or other immune cell functions in immune escape, new reports indicate that cancer cell-intrinsic PD-L1 potentially also modulate immune-independent cellular activities [8–12]. For example, some investigations suggested that cancer cell-intrinsic PD-L1 modulates glucose metabolism in sarcomas [13] and cell growth and autophagy in melanoma, ovarian and prostate cancers [14]. In the aforementioned mechanisms, PD-L1 functions through the phosphatidylinositol 3-kinase (PI3K)/serine/threonine kinase (AKT)/mechanistic target of rapamycin kinase (mTOR) network. Additionally, the aberrant PD-L1 expression has been demonstrated as a promising indicator for prognosis and chemotherapeutic response in patients with breast [15] and colorectal cancers [16]. Thus, targeting PD-L1 is crucial for chemotherapeutic sensitization through the inhibition of DNA damage repair [10]. In line, PD-L1 assessment in NSCLC cells allows to identify a patient population with higher likelihood of

recurrence and a decreased responsiveness to chemotherapy [10]. However, the potential mechanisms concerning the cell-intrinsic role of PD-L1 and its aberrant regulation in cancer biology and treatment have not been fully elucidated.

A growing body of evidence have revealed that the PD-L1 content is regulated by multiple cellular factors (e.g., growth factors, chemokines, oncogenes and tumor suppressor genes) at the transcriptional level. For example, interferon gamma (IFN- γ) is a strong activator of PD-L1 expression, and it employs the Janus kinase (JAK)/signal transducer and activator of transcription 1 (STAT1)/interferon regulatory factor 1 (IRF1) pathway in multiple types of human cancers, including NSCLC [17, 18]. Also, activating mutations involving *RAS* and epidermal growth factor receptor (*EGFR*) oncogenes are cancer-inducing and thus increase cancer cell-intrinsic PD-L1 levels via the PI3K-AKT and MAP kinase-ERK kinase (MEK)/extracellular regulated MAP kinase (ERK) networks in NSCLC cells [19, 20]. Nevertheless, there are limited reports on the molecular mechanisms behind the posttranslational modifications of PD-L1 [14]. The E3 ligases speckle type BTB/POZ protein (SPOP) and beta-transducin repeat-containing E3 ubiquitin protein ligase (β -TrCP) have been identified to ubiquitinate the PD-L1 protein and bring about its degradation in prostate [12, 21] and breast cancers [22]. Alternately, COP9 signalosome subunit 5 (CSN5), as a deubiquitinase, is upregulated by the tumor necrosis factor alpha (TNF- α)/nuclear factor-kappa B (NF- κ B) network in response to chronic inflammation, leading to PD-L1 protein stabilization and impairment of the anticancer therapy in breast cancer cells [23]. Therefore, a comprehensive understanding of the molecular mechanisms of PD-L1 posttranslational modulation can potentially aid in the development of novel and efficacious drugs that diminish PD-L1 protein content and overcome malignancy and therapeutic resistance in human cancers. In the present study, to ascertain whether a cancer cell-intrinsic role of PD-L1 is linked to the chemoresistant phenotypes in NSCLC, we performed a comprehensive study and jointly analyzed data from both in vitro and in vivo experimentations. Moreover, we sought to clarify the molecular processes underlying PD-L1 posttranslational regulation and its clinical relevance in NSCLC occurrence and progression.

2 | MATERIALS AND METHODS

2.1 | Cell culture

Human NSCLC cell lines A549 and PC9 and human embryonic kidney cell line 293T were acquired from

the American Type Culture Collection (Manassas, VA, USA), and cisplatin (DDP)-resistant A549^R and PC9^R cells from the Tianjin Medical University Cancer Institute and Hospital (Tianjin, China). All cells were verified to be mycoplasma negative via a GMyc-PCR mycoplasma test kit (Yeasen, Shanghai, China). A549 and PC9 cells were grown in RPMI-1640 (Gibco, Waltham, MA, USA), containing 10% fetal bovine serum (FBS) (Gibco) and 1% penicillin/streptomycin (ThermoFisher Scientific, Waltham, MA, USA). 293T cells were cultured in Dulbecco's Modified Eagle Medium (DMEM) (Gibco), containing 10% FBS, 1% sodium pyruvate (Gibco), 1% non-essential amino acids (NEAA) (Gibco) and 2% glutamine (Gibco). A549^R and PC9^R cells were cultured in RPMI-1640, containing 10% FBS, 1% penicillin/streptomycin and 2.5 μ mol/L DDP (Selleck, Houston, TX, USA).

2.2 | Reagents and drugs

PD-L1 neutralizing antibody avelumab (Selleck), the dosages were 2 μ g/mL in vitro and 5 mg/kg in vivo; the NF- κ B inhibitor Bay 11-7085 (TOPSCIENCE, Shanghai, China), the dosage was 5 μ mol/L in vitro; the protein synthesis inhibitor cycloheximide (CHX) (Selleck), the dosage was 100 μ g/mL in vitro; the chemotherapeutic drug DDP, the dosages were 5 μ mol/L in vitro and 5 mg/kg in vivo; the proteasomal inhibitor MG132 (Selleck), the dosage was 20 μ mol/L in vitro; the lysosomal inhibitor chloroquine (CQ) (Selleck), the dosage was 20 μ mol/L in vitro.

2.3 | Lentivirus-mediated knockdown and expression

Specific short hairpin RNAs (shRNAs) for PD-L1 and USP51 underwent annealing and subcloning into the pLV-H1-EF1 α -puro vector (Biosettia, San Diego, CA, USA). The full-length PD-L1 and USP51 as well as their deletion constructs (PD-L1-ET, PD-L1-TC, Flag-PD-L1-E, Flag-PD-L1-C, Flag-PD-L1-C1, Flag-PD-L1-C2, Flag-PD-L1-C3, Myc-USP51-N and Myc-USP51-C) (Sangon Biotech, Shanghai, China) underwent subcloning into the pLV-EF1-MCS-IRES-Bsd vector (Biosettia). The individual mutants of PD-L1 (K263R, K270R, K271R, K280R and K281R) (Sangon Biotech) also underwent subcloning into the pLV-EF1-MCS-IRES-Bsd vector. The constructed and packaged plasmids including gag polyprotein (Gag-Pol), regulator of expression of virion protein (Rev) and vesicular stomatitis virus glycoprotein G (VSVG) (Biosettia) were then co-incorporated into 293T cells with Lipofectamine 2000 reagent (Invitrogen, Waltham, MA, USA) to produce

lentivirus particles. The details of primers used can be found in Supplementary Table S1.

2.4 | RNA isolation and quantitative RT-PCR (qRT-PCR)

Total RNA was isolated with Trizol (Yeasen), followed by the first-strand cDNA generation using TransScript SuperMix (TransGen, Beijing, China). The chemoresistant genes were specifically amplified using quantitative PCR with SYBR Green Master Mix (Yeasen). The following PCR parameters were used: 95°C for 10 min, then 40 cycles of 95°C for 15 s, and 60°C for 1 min. The value of $\Delta\Delta C_t$ was employed to determine chemoresistant gene relative expression. Glyceraldehyde-3-phosphate dehydrogenase (GAPDH) served as a normalization control. The primer details can be found in Supplementary Table S1.

2.5 | Western blotting analysis

Total protein isolation and Western blotting was conducted as reported previously [24]. Protein samples were collected in lysis buffer for radio immunoprecipitation assay (RIPA) (Yeasen) with protease and phosphatase inhibitors (Yeasen), then quantified with a bicinchoninic acid (BCA) kit (ThermoFisher Scientific). Protein separation was performed with sodium dodecyl sulphate-polyacrylamide gel electrophoresis (SDS-PAGE) prior to transfer to polyvinylidene fluoride (PVDF) membranes (Millipore, Billerica, MA, USA), then blocked for 1 h in 5% skimmed milk (Yeasen) at room temperature, before overnight incubation with primary antibodies at 4°C with subsequent 1 h incubation in secondary antibodies at room temperature. Lastly, protein visualization employed enhanced chemiluminescence (ECL)-based chemiluminescence (Yeasen). A summary of the employed antibodies is available in Supplementary Table S2.

2.6 | Deubiquitination assay

Cells were incorporated with haemagglutinin (HA)-ubiquitin and the previously described plasmids, then treated with MG132 (Yeasen) for 6 h to inhibit ubiquitin-proteasome-dependent dysregulation of protein. Cell lysates were made in RIPA buffer (Yeasen), prior to overnight incubation in anti-Flag antibody or IgG at 4°C. The resulting immunoprecipitates were assayed using an anti-HA-Tag antibody-mediated Western blotting. The details of antibodies used can be found in Supplementary Table S2.

2.7 | Protein expression and purification for PD-L1 proteins

Glutathione S-transferase (GST)-tagged PD-L1 and its corresponding truncated mutants (GST-PD-L1-E, GST-PD-L1-IgV, GST-PD-L1-IgC2 and GST-PD-L1-C) (Sangon Biotech) underwent cloning into the pGEX-6p-1 vector (Biosettia) prior to expression in *E. coli* BL21 cells (WeiDi, Shanghai, China). Cell induction employed 0.5 mmol/L isopropyl β -D-thiogalactoside (IPTG) (Yeasen) in Luria-Bertani (LB) medium (Sigma, St. Louis, MO, USA) at 16°C for 24 h to induce PD-L1 protein expression. The cell pellet was dissolved in lysis buffer (50 mmol/L Tris, 300 mmol/L NaCl), and 2 mg/mL lysozyme (Yeasen) was added and incubated at 4°C overnight, followed by ultrasonication using Ultrasonic Crusher (SCIENTZ, Ningbo, Zhejiang, China), and a 20 min centrifugation at 18,000 \times g at 4°C. Following removal of supernatant, the inclusions were collected in solubilization buffer [200 mmol/L Tris, 5 mmol/L dithiothreitol (DTT), 8 mol/L urea, pH = 8.0]. Insoluble material was centrifuged at 18,000 \times g for 20 min at 4°C and removed, and the supernatant was placed onto Glutathione Sepharose 4B beads (ThermoFisher Scientific) and equilibrated with binding buffer (50 mmol/L Tris, 300 mmol/L NaCl) overnight. The protein was eluted with elution buffer (50 mmol/L Tris, 300 mmol/L NaCl, 10 mmol/L glutathione, pH = 7.5-8.0) and stored at -80°C.

2.8 | Coimmunoprecipitation and GST pulldown assays

Cell lysates were made in RIPA buffer, precleared using desired antibody or IgG at 4°C overnight, with subsequent incubation with protein G Resin (GenScript, Nanjing, Jiangsu, China) for 4 h. For GST pulldown assay, we incubated the cell lysates in GST-tagged proteins and Glutathione Sepharose 4B beads overnight at 4°C. Finally, the immunoprecipitates were separated with Western blotting with corresponding antibodies. The details of antibodies used can be found in Supplementary Table S2.

2.9 | In vitro binding assays

The purified proteins of histidine (His)-USP51 and GST-PD-L1 (full-length PD-L1 and its corresponding truncated mutants) were incubated at 4°C overnight. Glutathione Sepharose 4B beads were introduced and maintained for 4 h, before Western blotting of the bound proteins with USP51 antibody (H00158880-A01, Abnova, Taiwan, China).

2.10 | In vitro USP51 activity assay

C-terminal conjugate of ubiquitin with 7-amino-4-methylcoumarin (Ub-AMC) was used to measure the deubiquitinase activity of USP51. Briefly, the reaction system contained 50 mmol/L 2-hydroxyethyl, 0.5 mmol/L ethylene diamine tetraacetic acid, 100 mmol/L NaCl, 1 mmol/L DTT, 0.1 mg/mL bovine serum albumin, 64 nmol/L USP51 (MERRYBIO, Nanjing, Jiangsu, China) and 5 μ mol/L DHM (T2998, TOPSCIENCE) and was incubated at 37°C for 1 h. Then, 250 nmol/L Ub-AMC (U-550, BostonBiochem, Emeryville, CA, USA) was added, and the fluorescence intensity was detected using a microplate reader (BMG Labtech, Offenburg, Germany) with a 345 nm excitation/460 nm emission optic module for 3 h. All experiments had three biological replicates, and the mean value was analyzed.

2.11 | Surface plasmon resonance (SPR)

The binding kinetic evaluations were conducted on a Biacore T200 (GE Healthcare, Boston, MA, USA). Briefly, His-tagged USP51 were immobilized in Acetate 4.0 (BR-1003-49, GE Healthcare) on a Biacore Series S NTA chip (CM5) using N-terminal His tag capture, then amine-coupling with 1-(3-dimethylaminopropyl)-3-ethylcarbodiimide hydrochloride/N-hydroxy succinimide/ethanolamine (Sigma) as per kit guidelines. A 7500 response unit immobilization was attempted. Compounds were examined in two-fold dilution series in immobilization buffer containing 5% (V/V) dimethylsulfoxide (DMSO), at 30 μ L/min, with 60 s contact time and 120 s dissociation time. We also included a solvent correction curve between 4.5%-5.8% (V/V) DMSO. Ten-point dilution curves before and after compounds were used to confirm surface integrity throughout the experiment. The Biacore T200 Evaluation software (version 3.0, GE Healthcare) was employed with a kinetic fit.

2.12 | Cellular thermal shift assay

Cells underwent a 5 h DHM treatment at specified concentrations, then, they were accumulated for 3 min in PBS with a complete protease inhibitor cocktail, and respectively incubated at 40°C, 43°C, 46°C or 49°C. Next, cells were freeze-thawed in liquid nitrogen, and the supernatant was collected. Finally, proteins were assessed using Western blotting assay with USP51 antibody (SAB1305451, Sigma).

2.13 | Cell viability assessment

In all, 3,000 cells/well were plated in 96-well plates and treated with different drugs for different time points. Cell survivability was assessed via cell counting kit-8 (Yeasen), as per kit guidelines, using absorbance at 450 nm via a microplate reader (BMG Labtech).

2.14 | Colony formation experiment

In all, 750 cells/well were plated in 6-well plates before treatment with different drugs for 10 days. Cells underwent a 30 min fixation in 4% paraformaldehyde (Sigma), and 15 min crystal violet staining. The number of colonies was counted (colony formation rate = colony number/plated cell number).

2.15 | Flow cytometric analysis of cell apoptosis

Cells were treated with different drugs for 48 h before apoptotic assessment with the fluorescein isothiocyanate (FITC) Annexin-V/prodium iodide (PI) apoptosis detection kit (Yeasen) as per kit directions. Apoptotic cell percentage was evaluated using flow cytometry (LSR, BD Biosciences, San Diego, CA, USA).

2.16 | Immunofluorescence assay

Cells underwent 24-hour treatment with varying drugs before fixation in 4% paraformaldehyde, followed by overnight incubation with phosphorylated histone H2AX (γ H2AX) antibody (9718S, Cell Signaling Technology, Boston, MA, USA) at 4°C. The next day, cells were treated for 1 h with DyLight 594-conjugated secondary antibody (ab96885, abcam, Cambridge, Cambs, UK) before a 3 min staining with 4',6-diamidino-2-phenylindole (DAPI) (1 μ g/mL). The labeled nuclei were detected by Confocal FV1000 (Olympus, Tokyo, Japan). The percentage of cells with ≥ 10 foci was quantified. At least 100 cells were counted per well.

2.17 | Tumor xenograft experiment

All animal protocols received ethical approval from the Medical College of Nankai University (2021-SYDWLL-000040, Tianjin, China). We obtained 6-week-old male NOD-SCID mice from Beijing HFK Bioscience LTD (Beijing, China), and injected cells into their bilateral groins. Once tumors achieved a size of 50 mm³, mice were treated with different drugs for three weeks. When the tumor size

reached to approximately 800 mm³, the mice were euthanized following intraperitoneal anesthesia with ketamine and promethazine. The tumor weight was weighed, and volume was calculated as 1/2 (length × width²).

2.18 | Tissue microarray and immunohistochemistry (IHC)

Microarrays of human lung adenocarcinoma tissues (HLugA150CS03 and HLugA180Su04) were obtained from Shanghai Outdo Biotech Co., Ltd. (Shanghai, China). Samples underwent USP51, PD-L1 (17952-1-AP, Proteintech, Wuhan, Hubei, China) and ITGB1 (34971T, Cell Signaling Technology) antibody staining for IHC assays with the Envision Kit (Dako) in accordance as per kit protocols. Several pathologists then blindly scored the immunostaining, as described previously [24]. This protocol received ethical approval from the Nankai University (NKUIRB2021010).

2.19 | Bioinformatic analysis

The gene expression profiling interactive analysis (GEPIA) database (<http://gepia.cancer-pku.cn/>) was used to analyze the effect of ITGB1 on clinical survival. JASPAR (<http://jaspar.genereg.net/>) analysis was employed to identify a series of canonical NF- κ B response elements in the promoter region of chemoresistance-related genes.

2.20 | Statistical analysis

The experimental data were analyzed by GraphPad Prism 8.0 (GraphPad Software, San Diego, CA, USA) and SPSS 17.0 (IBM, Chicago, IL, USA) software (Chicago, IL, USA). Data from all experiments are expressed as mean ± standard deviation (SD) of three distinct replicates. Gene profile correlation in various samples were assessed via Spearman's rank correlation test. Inter-group comparison was performed using one-way analysis of variance (ANOVA). Unpaired data assessments were conducted using Student's *t*-test, as appropriate. *P* value < 0.05 was set as the significance threshold.

3 | RESULTS

3.1 | The extracellular domain of PD-L1 was required for the regulation of chemosensitivity in a cell-intrinsic manner

Consistent with previous report showing that abnormal PD-L1 content is involved in chemoresistance develop-

ment in human cancers [10], our Western blotting and flow cytometry assay results revealed a significant increase in PD-L1 levels in DDP-resistant A549^R cells compared to the wild-type A549 cells (Figure 1A). Thus, to further investigate the significance of cancer cell-intrinsic PD-L1 in chemoresistance, specific shRNAs targeting PD-L1 were introduced in A549^R followed by treatment with DDP. Based on our cell viability (Figure 1B), colony formation (Figure 1C) and cell apoptosis analyses (Figure 1D), PD-L1 depletion strongly promoted DDP-induced cell proliferation retardation and cell apoptosis. Similarly, the anti-apoptosis protein Bcl-2 was strongly diminished, whereas the pro-apoptosis proteins Bax and cleaved Caspase-3 were enhanced in shPD-L1/A549^R cells in response to DDP treatment (Supplementary Figure S1A). We also explored the effect of PD-L1 on DDP-induced γ H2AX expression, which is a marker for DNA damage repair [25]. The results confirmed that PD-L1 knockdown significantly enhanced DDP-induced formation of γ H2AX nuclear foci (Figure 1E) and the level of γ H2AX expression (Supplementary Figure S1B). Consistently, we obtained the similar results in shPD-L1/PC9^R cells (Supplementary Figure S2), indicating that cell-intrinsic PD-L1 potentially modulates chemosensitivity in NSCLC cells.

Further, we determined whether aberrant PD-L1 content influenced tumor responsiveness to chemotherapeutic treatment in vivo. To do so, shPD-L1/A549^R or shCtrl/A549^R cells were subcutaneously injected into BALB/c nude mice to develop a tumor xenograft model, which was then treated with DDP. Based on our observation, DDP strongly suppressed tumor development in BALB/c nude mice with shPD-L1/A549^R tumors as compared to shCtrl/A549^R tumors (Figure 1F-G). Immunohistochemical staining further demonstrated that DDP treatment resulted in decreased Ki67 expression but increased cleaved Caspase-3 and γ H2AX expression in shPD-L1/A549^R tumors as compared to shCtrl/A549^R tumors (Figure 1H). Thus, the above observations confirmed the involvement of aberrant PD-L1 in NSCLC chemoresistance, independent of the immune system in vitro and in vivo.

Next, to elucidate the functional domain of PD-L1 that contributes to its cell-intrinsic role in chemoresistance, the full-length PD-L1 (PD-L1-FL) and two deletion constructs PD-L1-ET (containing the extracellular and transmembrane domains of PD-L1) and PD-L1-TC (containing the transmembrane and cytoplasmic domains of PD-L1) were generated and overexpressed in A549 cells (Figure 1I). The cell viability (Figure 1J), colony formation (Figure 1K), cell apoptosis (Figure 1L and Supplementary Figure S3A), and DNA damage detection assays (Figure 1M and Supplementary Figure S3B) confirmed that overexpression of PD-L1-FL strongly reduced cell proliferation retarda-

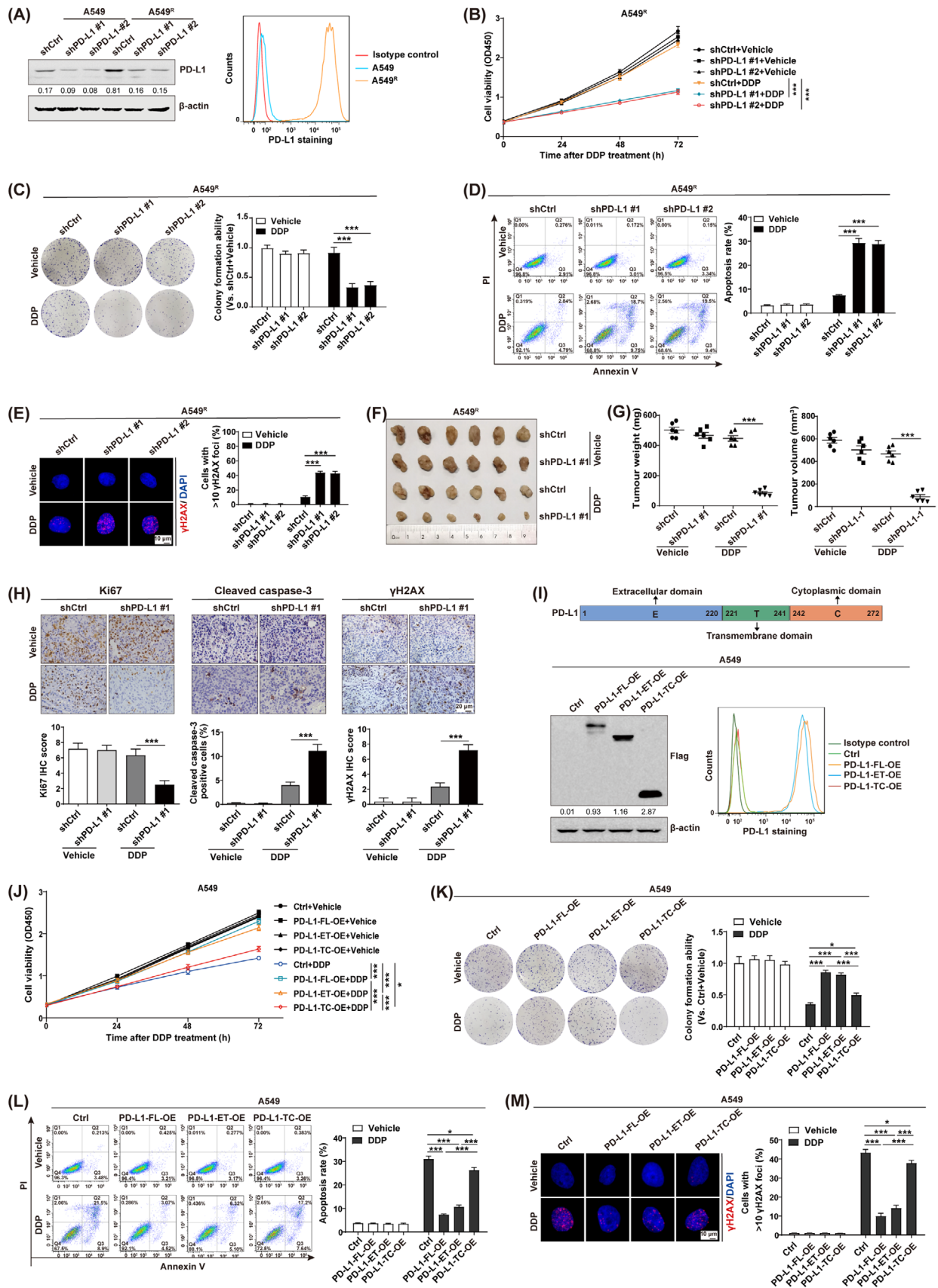


FIGURE 1 The PD-L1 extracellular domain is required for the regulation of chemosensitivity in a cell-intrinsic manner in NSCLC. (A) PD-L1 expression, as evidenced by Western blotting and flow cytometry in shCtrl/A549^R and shPD-L1/A549^R cells. (B-E) The analyses of cell viability (B), colony formation (C), cell apoptosis (D) and γ H2AX foci formation (E) were examined in shCtrl/A549^R and shPD-L1/A549^R cells

tion and cell apoptosis and decreased the formation of γ H2AX nuclear foci upon DDP treatment. Notably, we found that overexpression of PD-L1-ET showed a similar effect to attenuate cancer cell responsiveness to DDP. We observed the same alterations in PC9 cells (Supplementary Figure S4), indicating that the PD-L1 extracellular domain conferred the regulation of chemosensitivity through a cell-intrinsic mechanism in NSCLC cells.

3.2 | ITGB1 mediated PD-L1-induced chemoresistance

In addition, we moved to identify the downstream signaling pathway that mediated PD-L1-induced chemoresistance in NSCLC cells. Surprisingly, treatment with the PD-L1 neutralizing antibody avelumab did not show a chemosensitizing effect by the analysis of cell viability (Supplementary Figure S5A), colony formation (Supplementary Figure S5B), cell apoptosis (Supplementary Figure S5C-D), and DNA damage detection (Supplementary Figure S5E-F) in A549^R cells. Considering that a complex structure analysis revealed an IgV-dominated binding pattern between PD-L1 and its neutralizing antibody [26], these results highlight that the cancer cell-intrinsic role of PD-L1 in chemoresistance might be independent of its interaction with the PD-1 receptor through the IgV domain. Consequently, we performed an endogenous Co-IP combining with mass spectrometry and identified several cell membrane-bound receptors that could potentially interact with PD-L1 in A549^R cells (Supplementary Figure S6A). Quantitative RT-PCR further demonstrated a significant upregulation of ITGB1, CD98 and CD44 expression in A549^R cells (Supplementary Figure S6B). Of note, the GEPIA database analysis revealed that elevated ITGB1 levels were closely related to shorter overall survival (OS) (Supplementary Figure S6C) and disease-free survival (Supplementary Figure S6D) in NSCLC patients.

Importantly, the Co-IP assay demonstrated an increased physical interaction between PD-L1 and ITGB1 in A549^R cells relative to A549 cells (Figure 2A). Moreover, cell viability (Figure 2B), colony formation (Figure 2C), cell apoptosis (Figure 2D and Supplementary Figure S7A), and

DNA damage detection assays (Figure 2E and Supplementary Figure S7B) demonstrated that either PD-L1 depletion or ITGB1 neutralization significantly promoted cancer cell chemosensitivity to DDP in A549^R cells; however, the combinatorial treatment did not elicit a synergistic anticancer activity. Similarly, we conducted the same investigations in PC9^R cells and achieved comparable results (Supplementary Figure S8).

Next, we identified the PD-L1 functional domain that mediates its association with ITGB1. We constructed three GST fusion proteins for the extracellular domain of PD-L1 (PD-L1-E, PD-L1-IgV and PD-L1-IgC2). The results of GST-pulldown assay confirmed that PD-L1 physically interacted with ITGB1 through its extracellular domain (Figure 2F). Of note, the deletion variant PD-L1-IgC2, but not PD-L1-IgV, was able to interact with ITGB1. Taken together, our data proposed that ITGB1 specifically functioned as a membrane-binding receptor for PD-L1 and thus mediates its cell-intrinsic role in chemoresistant NSCLC cells.

3.3 | PD-L1 conferred chemoresistance by triggering the ITGB1/NF- κ B signaling

Next, we moved to identify the molecular mechanism of PD-L1/ITGB1-regulated cancer cell responsiveness to chemotherapy in NSCLC. Of note, TCGA database analysis revealed that the transcript levels of multiple chemoresistance-related genes, such as baculoviral IAP repeat containing 5 (*BIRC5*) [27], breast cancer gene 1 (*BRCA1*) [28, 29], *BRCA2* [30, 31], glutathione synthetase (*GSS*) [32], hypoxia inducible factor 1 alpha (*HIF1 α*) [33], and solute carrier family 31 member 2 (*SLC31A2*) [34], were positively correlated with those of *PD-L1* (Supplementary Figure S9A) and *ITGB1* (Supplementary Figure S9B) in NSCLC patients. Quantitative RT-PCR further verified that expression of these chemoresistance-related genes was significantly downregulated by either PD-L1 depletion or ITGB1 neutralization in A549^R cells (Figure 3A). However, the combinatorial treatment did not exhibit a synergistic inhibition, which is consistent with our notion that PD-L1-promoted chemoresistance is mainly mediated through its binding to the ITGB1

following treatment with DDP (5 μ mol/L) or vehicle. (F) shCtrl/A549^R and shPD-L1/A549^R cells were subcutaneously administered to NOD-SCID mice following treatment with DDP (5 mg/kg). (G) The tumor weight and volume are shown. (H) The Ki67, cleaved Caspase-3 and γ H2AX contents, as examined by immunohistochemical staining in xenograft tumors. (I) The PD-L1 levels, as detected by Western blotting and flow cytometry in Ctrl/A549, PD-L1-FL/A549, PD-L1-ET/A549 and PD-L1-TC/A549 cells. (J-M) The analyses of cell viability (J), colony formation (K), cell apoptosis (L) and γ H2AX foci formation (M) were examined in Ctrl/A549, PD-L1-FL/A549, PD-L1-ET/A549 and PD-L1-TC/A549 cells in response to DDP. **P* < 0.05, ****P* < 0.001; (B) and (J) were assessed via two-way ANOVA with Sidak correction for multiple comparisons; (C-E), (G-H) and (L-M) were assessed via unpaired Student's *t*-test. Abbreviations: NSCLC, non-small cell lung cancer; DDP, cisplatin; PD-L1, programmed death ligand 1; γ H2AX, phosphorylated histone H2AX; ANOVA, analysis of variance.

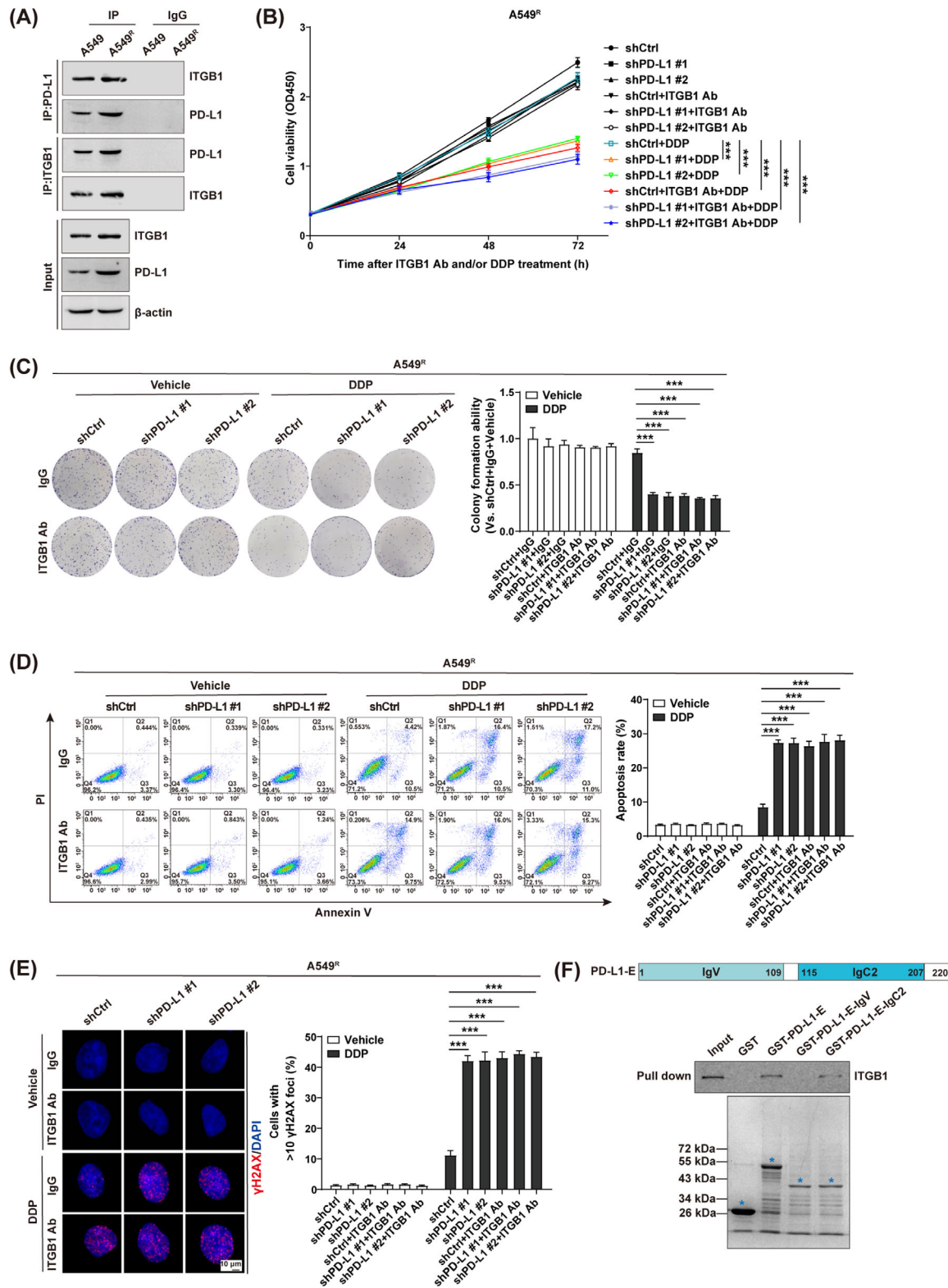


FIGURE 2 ITGB1 mediates PD-L1-induced chemoresistance. (A) The interaction between PD-L1 and ITGB1 was detected using Co-IP assay in A549 and A549^R cells. (B-E) The analyses of cell viability (B), colony formation (C), cell apoptosis (D) and γ H2AX foci formation (E) were examined in shCtrl/A549^R and shPD-L1/A549^R cells following treatment with ITGB1 neutralizing antibody (2 μ g/mL) and/or DDP (5 μ mol/L). (F) The interaction between ITGB1 and the deletion mutants GST-PD-L1-E, GST-PD-L1-E-IgV and GST-PD-L1-E-IgC2 was examined by GST pull-down assay in A549^R cells. *** P < 0.001; (B) was assessed via two-way ANOVA with Sidak correction for multiple comparisons; (C-E) were analyzed by unpaired Student's t -test. Abbreviations: ITGB1, integrin beta 1; Co-IP, coimmunoprecipitation; ITGB1 Ab, ITGB1 neutralizing antibody; DDP, cisplatin; GST, glutathione S-transferase; PD-L1, programmed death ligand 1; γ H2AX, phosphorylated histone H2AX; ANOVA, analysis of variance.

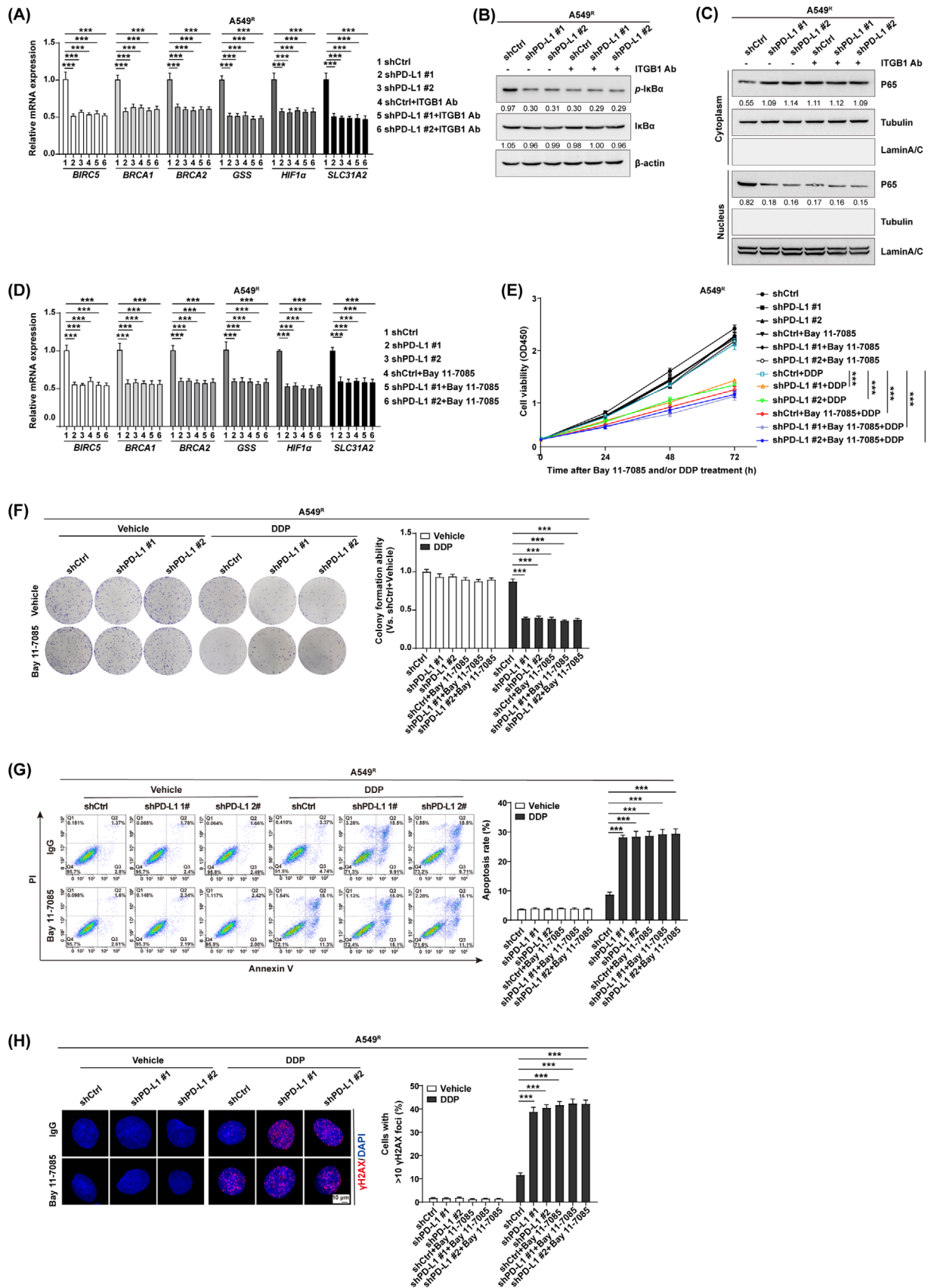


FIGURE 3 PD-L1 confers chemoresistance by triggering the ITGB1/NF- κ B signaling. (A) The transcript levels of multiple chemoresistance-associated genes (*BIRC5*, *BRCA1*, *BRCA2*, *GSS*, *HIF1 α* and *SLC31A2*) as evidenced by quantitative RT-PCR in shCtrl/A549^R and shPD-L1/A549^R cells following treatment with ITGB1 neutralizing antibody. (B-C) The protein levels of phospho-I κ B α (B) and NF- κ B/P65

receptor on NSCLC cells. Interestingly, analysis using the JASPAR database identified a series of canonical NF- κ B response elements in the promoter region of all above chemoresistance-related genes (Supplementary Figure S9C), indicating a potential role of the NF- κ B signaling in PD-L1/ITGB1-regulated chemoresistance [35]. Thus, expression of the NF- κ B components was assessed via Western blotting in shPD-L1/A549^R cells with or without ITGB1 neutralizing antibody. We confirmed that either PD-L1 knockdown or ITGB1 neutralization could reduce the expression of phosphorylated I κ B α (Figure 3B), with a simultaneous decrease in the nuclear transfer of the P65 subunit (Figure 3C). However, a synergistic inhibition in the NF- κ B signaling was not achieved by the combinational treatment.

In line, the quantitative RT-PCR (Figure 3D), cell viability (Figure 3E), colony formation (Figure 3F), cell apoptosis (Figure 3G and Supplementary Figure S10A), and DNA damage detection (Figure 3H and Supplementary Figure S10B) assays further revealed that either depletion of PD-L1 or treatment with an NF- κ B inhibitor Bay 11-7085 increased A549^R cell chemosensitivity to DDP; however, we did not observe a synergistic suppression with the combinational treatment. Similar results were also obtained in PC9^R cells (Supplementary Figure S11), confirming that the PD-L1/ITGB1 axis promoted NSCLC cell sensitivity to chemotherapy by triggering the NF- κ B signaling.

3.4 | USP51 promoted chemoresistance through deubiquitination of PD-L1

To further explore if the abnormal PD-L1 content is related to posttranslational modulation in chemoresistant NSCLC cells, we next treated A549^R and A549 cells with the protein synthesis inhibitor CHX. Western blotting analysis demonstrated that the stability of PD-L1 protein was strongly enhanced in A549^R cells relative to A549 cells (Supplementary Figure S12A). Moreover, exposure to the proteasomal inhibitor MG132 (Supplementary Figure S12B) and not the

lysosomal inhibitor CQ (Supplementary Figure S12C) led to remarked upregulation of PD-L1 protein. The ubiquitination assay data revealed that the polyubiquitination level of PD-L1 protein was strongly decreased upon MG132 treatment in A549^R cells compared to that in A549 cells (Supplementary Figure S12D). Also, we confirmed these results in PC9^R and PC9 cells (Supplementary Figure S13). These data indicated a ubiquitin proteasome-dependent dysregulation of PD-L1 content in chemoresistant NSCLC cells.

Notably, the analysis of endogenous Co-IP combining with mass spectrometry identified two deubiquitinases [USP51 and ubiquitin C-terminal hydrolase L1 (UCHL1)] and two E3 ubiquitin ligases [ring finger protein 31 (RNF31) and tripartite motif containing 21 (TRIM21)] that could potentially interact with PD-L1 in A549^R cells (Supplementary Figure S14A). We further validated the physical interactions of PD-L1 with USP51 (Figure 4A), UCHL1 (Supplementary Figure S14B), RNF31 (Supplementary Figure S14C), and TRIM21 (Supplementary Figure S14D) in PD-L1-overexpressing A549 cells. However, Western blotting and flow cytometry assays demonstrated that the specific interference of USP51 (Figure 4B), but not UCHL1 (Supplementary Figure S14E), RNF31 (Supplementary Figure S14F) and TRIM21 (Supplementary Figure S14G), altered PD-L1 levels in A549^R cells. Western blotting data revealed that the expression of USP51 was significantly elevated in A549^R cells (Figure 4C). These observations demonstrated a predominant function of USP51 in the posttranslational modulation of PD-L1 in chemoresistant NSCLC cells. In line, the PD-L1 protein stability was strongly decreased upon CHX treatment in shUSP51/A549^R cells (Figure 4D). However, USP51-interfered PD-L1 content decrease was strongly weakened with MG132 addition (Figure 4E). Based on our ubiquitination assay, USP51 depletion strongly enhanced PD-L1 protein polyubiquitination in A549^R cells (Figure 4F), collectively suggesting that USP51, a deubiquitinase, targeted PD-L1 protein for deubiquitination and stabilization. Similar results were further obtained in PC9^R cells (Supplementary Figure S15).

subunit (C) were detected by Western blotting in shCtrl/A549^R and shPD-L1/A549^R cells following treatment with ITGB1 neutralizing antibody. (D) The transcript levels of multiple chemoresistance-associated genes (*BIRC5*, *BRCA1*, *BRCA2*, *GSS*, *HIF1 α* and *SLC31A2*) as evidenced by quantitative RT-PCR in shCtrl/A549^R and shPD-L1/A549^R cells following treatment with an NF- κ B inhibitor Bay 11-7085 (5 μ mol/L). (E-H) The evaluations of cell viability (E), colony formation (F), cell apoptosis (G) and γ H2AX foci formation (H) were examined in shCtrl/A549^R and shPD-L1/A549^R cells following treatment with Bay 11-7085 and/or DDP. *** P < 0.001; (E) was analyzed via two-way ANOVA with Sidak correction for multiple comparisons; (A), (D) and (F-H) were assessed via unpaired Student's t -test. Abbreviations: ITGB1, integrin beta 1; NF- κ B, nuclear factor-kappa B; ITGB1 Ab, ITGB1 neutralizing antibody; BIRC5, baculoviral IAP repeat containing 5; BRCA1, breast cancer gene 1; BRCA2, breast cancer gene 2; GSS, glutathione synthetase; HIF1 α , hypoxia inducible factor 1 alpha; SLC31A2, solute carrier family 31 member 2; DDP, cisplatin; RT-PCR, real time-polymerase chain reaction; PD-L1, programmed death ligand 1; γ H2AX, phosphorylated histone H2AX; ANOVA, analysis of variance.

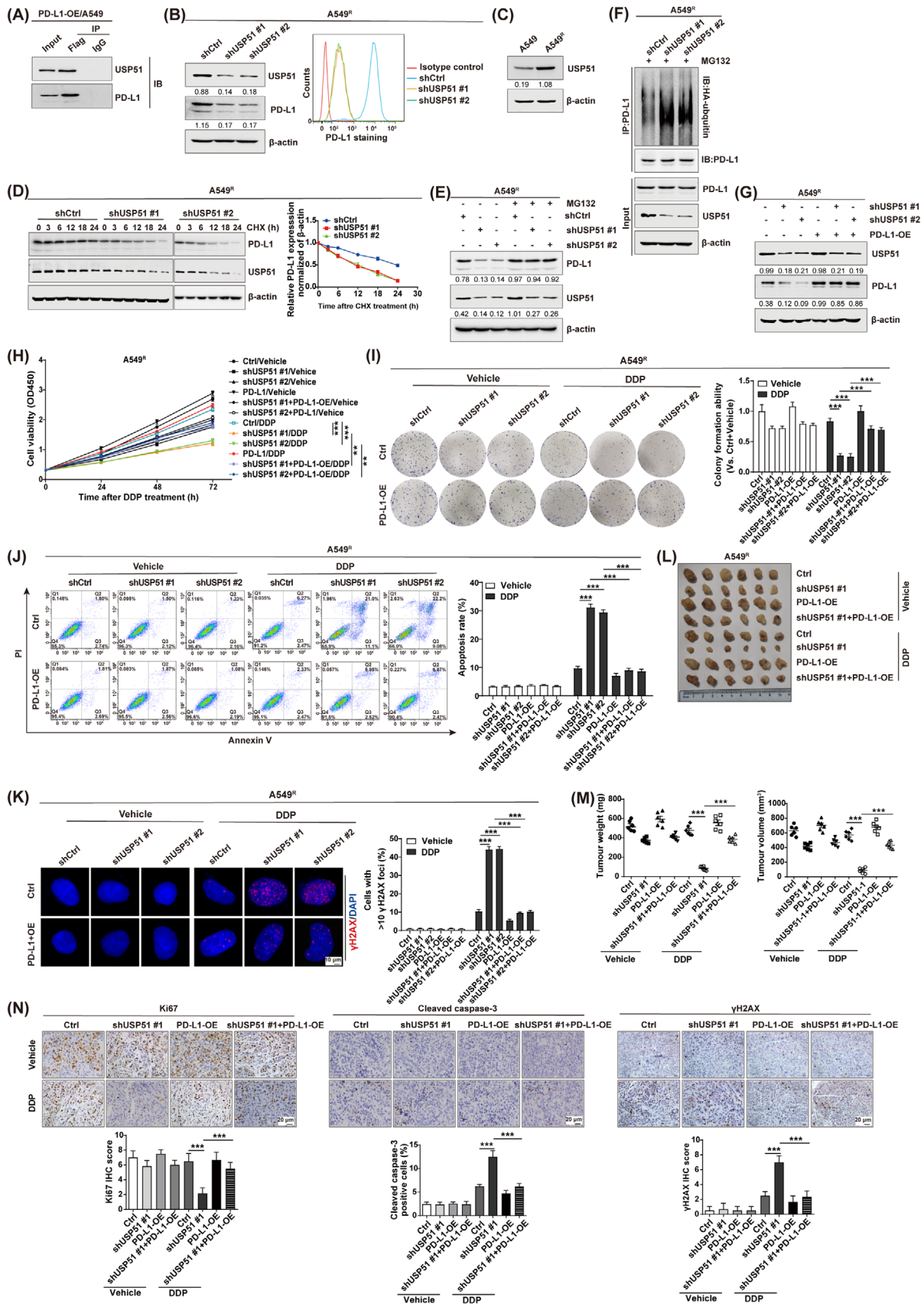


FIGURE 4 USP51 promotes chemoresistance through deubiquitination of PD-L1. (A) The association between USP51 and PD-L1 was detected by Co-IP assay in PD-L1/A549 cells. (B) USP51 and PD-L1 expression as evidenced by Western blotting and flow cytometry in shCtrl/A549^R and shUSP51/A549^R cells. (C) USP51 expression as evidenced by Western blotting in A549 and A549^R cells. (D) The stability of

Next, we examined whether USP51 depletion could chemosensitize NSCLC cells through the regulation of PD-L1. To do so, PD-L1 was overexpressed in shUSP51/A549^R cells (Figure 4G). The cell viability (Figure 4H), colony formation (Figure 4I), cell apoptosis (Figure 4J and Supplementary Figure S16A), and DNA damage detection assays (Figure 4K and Supplementary Figure S16B) demonstrated that cell responsiveness to chemotherapy was increased in shUSP51/A549^R cells; nevertheless, this outcome was strongly diminished in PD-L1-overexpressed cells. We observed comparable results in PC9^R cells (Supplementary Figure S17). In line, using BALB/c nude mice xenograft model, we confirmed that USP51 knockdown severely inhibited tumor growth upon DDP treatment, which was suppressed in mice with PD-L1-harboring tumors (Figure 4L-M). Immunohistochemical staining further indicated that the Ki67 content was diminished but the cleaved Caspase-3 and γ H2AX contents were increased in tumors from shUSP51/A549^R mice when treated with DDP, and this outcome was suppressed in tumors with PD-L1 rescue (Figure 4N). These observations together revealed that USP51 deficiency chemosensitized NSCLC cells via PD-L1 regulation both in vitro and in vivo.

3.5 | USP51 deubiquitinated PD-L1 at lysine residues K280/K281

Consequently, we conducted an endogenous Co-IP to validate the USP51 and PD-L1 relationship. The results revealed that USP51 directly associated with PD-L1 in A549 cells, which was further increased in A549^R cells (Figure 5A). Importantly, an in vitro binding assay proved that the purified proteins of His-USP51 and GST-PD-L1 could directly associate with one another in cell-free environment (Figure 5B). Moreover, a series of deletion mutants of USP51 (Myc-USP51-N and Myc-USP51-C) and PD-L1 (Flag-PD-L1-E and Flag-PD-L1-C) were generated and overexpressed in A549 cells. Our Co-IP data verified that the deletion variant Myc-USP51-N interacted with

the PD-L1 cytoplasmic domain (Figure 5C-D). In addition, three deletion constructs of PD-L1-C were generated to demonstrate that the deletion variant PD-L1-C3, but not PD-L1-C1 and PD-L1-C2, was able to interact with USP51 (Figure 5E), highlighting that the PD-L1C-terminal region (280-290aa) is critical for the USP51-PD-L1 association.

Next, we examined whether USP51 could deubiquitinate the lysine residues of PD-L1-C3. As shown in Figure 5F, the wild-type and individual mutants of PD-L1 (K263R, K270R, K271R, K280R and K281R) were respectively transfected into shUSP51/A549^R cells. The ubiquitination assay indicated that the polyubiquitination levels of either K280R or K281R was significantly reduced compared to wild-type PD-L1, however this effect was not shown for the K263R, K270R and K271R mutants. In addition, the simultaneous mutant K280R+K281R totally abolished the polyubiquitination levels of PD-L1 (Figure 5G), identifying lysine residues K280 and K281 as major ubiquitination sites on PD-L1. Indeed, USP51 was able to deubiquitinate PD-L1 at either K280 or K281 lysine residue (Figure 5H). The interference of USP51 led to a strongly reduced stability of wild-type PD-L1 protein; however, this effect was deprived in cells carrying the simultaneous mutant K280R+K281R (Figure 5I). The same experiments were also conducted in PC9^R cells and produced comparable results (Supplementary Figure S18). Taken together, our data demonstrated that lysine residues K280 and K281 on the PD-L1 C-terminal region were essential for its deubiquitination and stabilization by USP51 in chemoresistant NSCLC cells.

3.6 | The USP51, PD-L1 and ITGB1 contents were positively associated with worse prognosis among NSCLC patients

To further validate the pathological relationship between the USP51/PD-L1/ITGB1 axis and chemoresistant features in human NSCLC, we conducted immunohistochemical staining for USP51, PD-L1 and ITGB1 in 167 samples of primary NSCLC (Figure 6A). We observed direct relation-

PD-L1 protein was detected by CHX pulse-chase analysis in shCtrl/A549^R and shUSP51/A549^R cells. Data normalized to β -actin levels. (E) PD-L1 and USP51 expression as evidenced by Western blotting in shCtrl/A549^R and shUSP51/A549^R cells with or without MG132. (F) PD-L1 protein ubiquitination as evidenced by Co-IP assay in shCtrl/A549^R and shUSP51/A549^R cells. (G) USP51 and PD-L1 expression as detected by Western blotting in shCtrl/A549^R and shUSP51/A549^R cells with PD-L1 rescue. (H-K) The analyses of cell viability, colony formation (I), cell apoptosis (J) and γ H2AX foci formation (K) were examined in shCtrl/A549^R and shUSP51/A549^R cells with PD-L1 rescue following treatment with DDP. (L) shCtrl/A549^R and shUSP51/A549^R cells with PD-L1 rescue were subcutaneously injected into NOD-SCID mice following treatment with DDP. (M) The tumor weight and volume are shown. (N) Ki67, cleaved caspase-3 and γ H2AX contents as examined by immunohistochemical staining in xenograft tumors. ** $P < 0.01$, *** $P < 0.001$; (H) was analyzed via two-way ANOVA with Sidak correction for multiple comparisons; (I-K) and (M-N) were assessed via unpaired Student's *t*-test. Abbreviations: Co-IP, coimmunoprecipitation; CHX, Cycloheximide; DDP, cisplatin; PD-L1, programmed death ligand 1; USP51, ubiquitin-specific peptidase 51; γ H2AX, phosphorylated histone H2AX; ANOVA, analysis of variance.

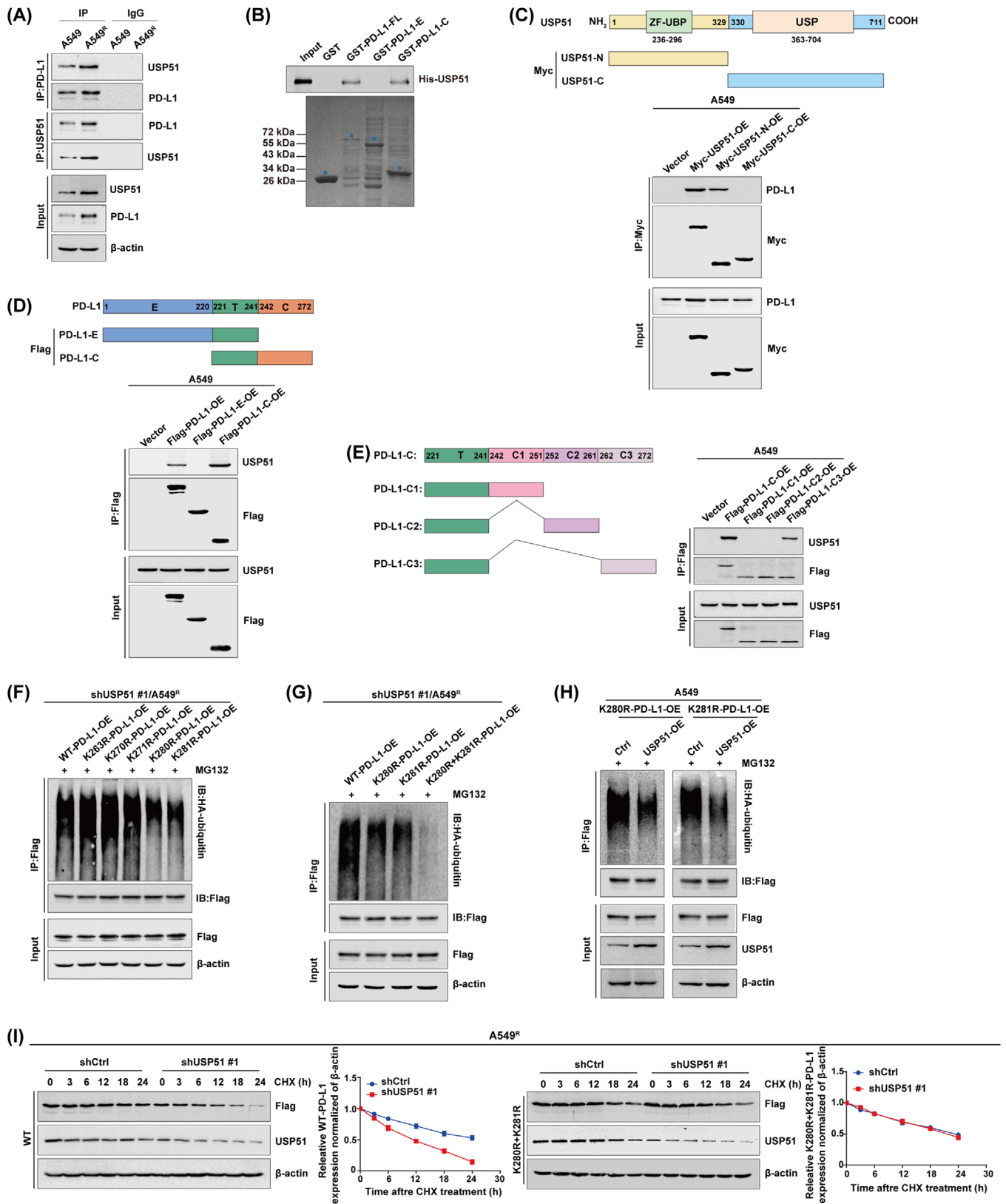


FIGURE 5 USP51 deubiquitinates PD-L1 at lysine residues K280/K281. (A) The interaction between PD-L1 and USP51 as detected via Co-IP assay in A549 and A549^R cells. (B) The association between His-USP51 and the purified recombinant proteins of GST-PD-L1-ETC, GST-PD-L1-E and GST-PD-L1-C was detected by in vitro binding assay. (C) The physical association between PD-L1 and wild-type or deletion mutants of USP51 (Myc-USP51-N and Myc-USP51-C) was detected by Co-IP assay in A549 cells. (D) The association between USP51 and wild-type or deletion mutants of PD-L1 (Flag-PD-L1-E and Flag-PD-L1-C) was detected by Co-IP assay in A549 cells. (E) The association

ships between USP51, PD-L1 and ITGB1 (Figure 6B). It has been reported that Cyclin D1 [36, 37] and breast cancer gene 1 (BRCA1) [38, 39], which mediate cell proliferation and DNA damage response, respectively, were strongly elevated in NSCLC tissues resistant to genotoxic drugs. Indeed, we revealed that the USP51, PD-L1 and ITGB1 contents were intricately linked to Cyclin D1 (Figure 6C) and BRCA1 (Figure 6D), highlighting the involvement of aberrant USP51/PD-L1/ITGB1 expression in the cellular mechanisms that mediated NSCLC chemoresistance.

In addition, we observed increased USP51, PD-L1 and ITGB1 levels in high-grade tumors (Figure 6E) and advanced tumor-node-metastasis (TNM) stage (Figure 6F). Of note, the cancer patients with substantially elevated USP51, PD-L1 and ITGB1 levels in tumors exhibited shorter OS relative to patients with reduced USP51, PD-L1 and ITGB1 contents (Figure 6G). We also examined OS of the triple-high group (USP51^{high}PD-L1^{high}ITGB1^{high}) compared to the rest (Figure 6H). The results confirmed that patients with concomitantly high expression of USP51, PD-L1 and ITGB1 in tumors had significantly shorter OS (Figure 6I). Taken together, these data revealed that dysregulation of the USP51/PD-L1/ITGB1 axis potentially contributes to the malignant progression and may be employed in the prediction of worse NSCLC patient prognosis.

3.7 | Dihydromyricetin acted as a USP51 inhibitor and conferred chemosensitization in NSCLC

Next, we moved to identify the small molecules that could potentially alter USP51 activity. To do so, we used the fluorescent Ub-AMC assay to examine an in-house library containing 188 natural compounds (Figure 7A and Supplementary Table S3). Five compounds, dihydromyricetin (DHM), (-)-epigallocatechin (EGC), gallic acid, linoleic acid, and tannic acid, were shown to significantly inhibit the deubiquitinase activity of USP51 at a concentration of 1 μ mol/L (Supplementary Table S4). Further, we conducted a computational molecular dynamics simulation and revealed that three flavonoid compounds DHM, EGC

and gallic acid could potentially bind to the catalytic domain of USP51 (Figure 7B). Of note, the analysis of half maximal inhibitory concentration (IC₅₀) indicated that DHM performed a stronger inhibition in USP51 activity than EGC and gallic acid (Figure 7C). In line with this, the SPR binding assay validated a significantly increased binding affinity between USP51 and DHM (Figure 7D). Taken together with the cellular thermal shift assay showing that DHM treatment effectively stabilized USP51 protein in A549^R (Figure 7E) and PC9^R cells (Supplementary Figure S19), our results indicated that DHM might target USP51 directly.

In addition, to examine whether DHM exerted its biological function through a USP51-dependent mechanism, we introduced the full-length USP51 into A549 cells followed by treatment with DHM (Supplementary Figure S20A). Based on our Western blotting results, the PD-L1 content was upregulated in USP51-OE/A549 cells, whereas this effect was significantly abolished by DHM treatment. Consistently, the ubiquitination assay revealed that USP51 deubiquitinase inhibition by treatment with DHM led to increased polyubiquitination of PD-L1 proteins in USP51/A549 cells (Supplementary Figure S20B). The cell viability (Supplementary Figure S20C), colony formation (Supplementary Figure S20D), cell apoptosis (Supplementary Figure S20E-F), and DNA damage detection assays (Supplementary Figure S20G-H) further confirmed that overexpression of USP51 strongly reduced cell proliferation retardation and cell apoptosis but promoted DNA damage repair in response to DDP; however, USP51-induced chemoresistant phenotypes were weakened by the addition of DHM. Similar results were also obtained in PC9 cells (Supplementary Figure S21), highlighting a role of DHM in the regulation of chemosensitization via targeting USP51.

Indeed, treatment with DHM strongly promoted DDP-induced cell proliferation retardation (Figure 7F-G) and cell apoptosis (Figure 7H and Supplementary Figure S22A) in A549^R cells, while this effect was impaired by USP51 interference. We also examined the effect of DHM on DDP-induced DNA damage response with or without USP51 depletion (Figure 7I and Supplementary Figure S22B), revealing that DHM conferred responsiveness to

between USP51 and deletion mutants of PD-L1-C (Flag-PD-L1-C1, Flag-PD-L1-C2 and Flag-PD-L1-C3) was detected via Co-IP assay in A549 cells. (F) PD-L1 protein ubiquitination as evidenced via Co-IP assay in shUSP51/A549^R cells with overexpression of wild-type or site-directed mutants of PD-L1 (K263R-PD-L1, K270R-PD-L1, K271R-PD-L1, K280R-PD-L1 and K281R-PD-L1). (G) PD-L1 protein ubiquitination as evidenced by Co-IP assay in shUSP51/A549^R cells with overexpression of wild-type or site-directed mutants of PD-L1 (K280R-PD-L1, K281R-PD-L1 and K280R+K281R-PD-L1). (H) The ubiquitination of PD-L1 protein was detected by Co-IP assay in K280R-PD-L1/A549 and K281R-PD-L1/A549 cells with overexpression of USP51. (I) The stability of WT-PD-L1 or K280R+K281R-PD-L1 protein was detected by CHX pulse-chase analysis in shCtrl/A549^R and shUSP51/A549^R cells. Data normalized to β -actin levels. Abbreviations: Co-IP, coimmunoprecipitation; GST, glutathione S-transferase; CHX, Cycloheximide; PD-L1, programmed death ligand 1; USP51, ubiquitin-specific peptidase 51.

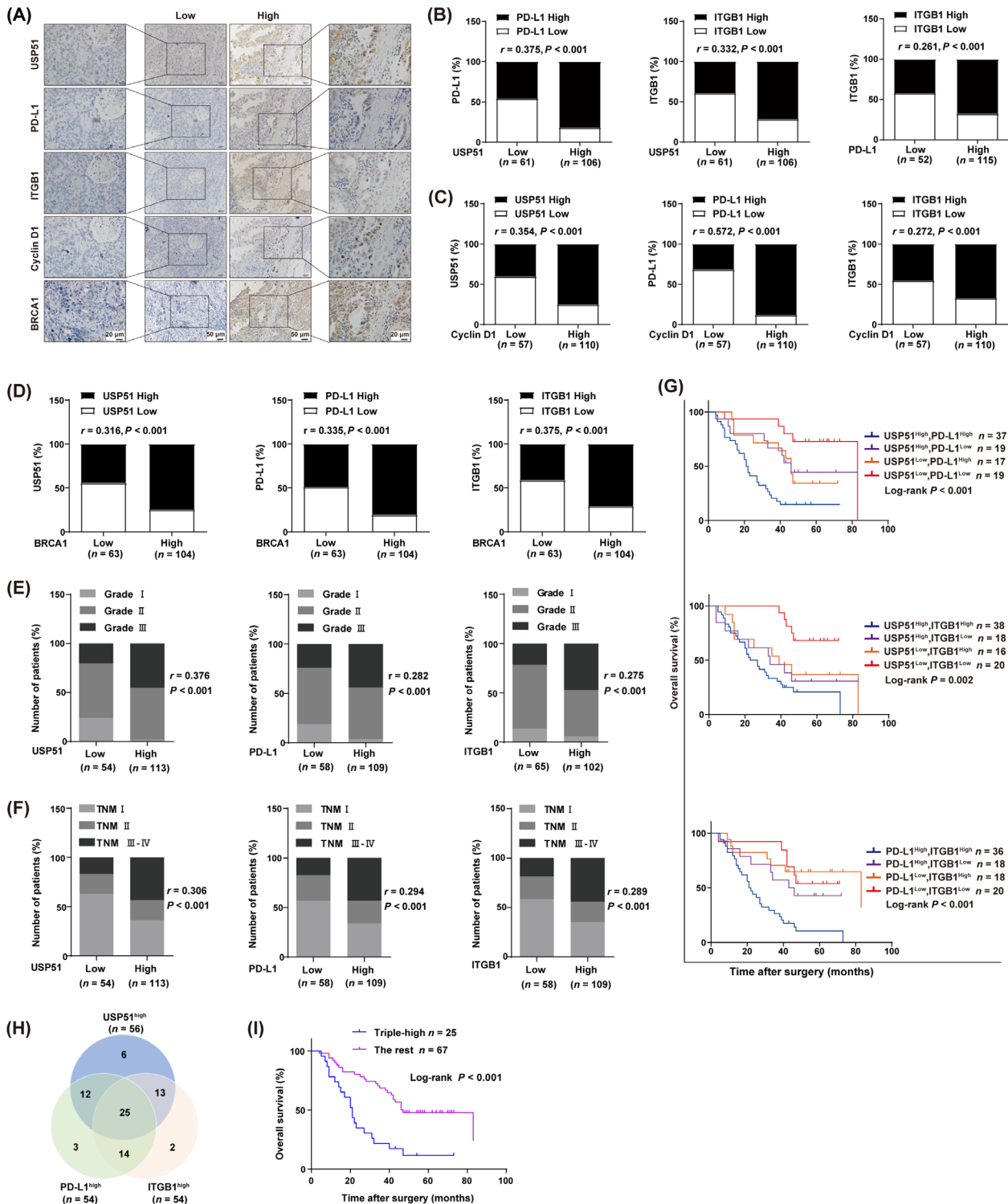


FIGURE 6 USP51, PD-L1 and ITGB1 expressions are associated with worse prognosis in NSCLC patients. (A) Immunohistochemical staining images of USP51, PD-L1 and ITGB1 from serial sections of the same tumor from two distinct cases. (B) A direct association between the USP51, PD-L1 and ITGB1 expressions in 167 human NSCLC samples. (C) A positive association between the USP51, PD-L1, ITGB1 and Cyclin D1 expressions in 167 human NSCLC samples. (D) A positive association between the USP51, PD-L1, ITGB1 and BRCA1 expressions in 167 human NSCLC samples. (E) A positive association between the USP51, PD-L1 and ITGB1 expressions and pathological grade. (F) A direct association between the USP51, PD-L1 and ITGB1 contents and with advanced TNM stage. (G) Kaplan-Meier survival curves of overall survival in patients with elevated or reduced expression of USP51, PD-L1 and ITGB1. (H) The Venn diagram in patients with high expression of USP51, PD-L1 and ITGB1. (I) The overall survival of the triple-high group (USP51^{high}PD-L1^{high}ITGB1^{high}) and rest group. (B-F) were assessed via Spearman's rank correction test; (G) and (I) were analyzed by log-rank test. Abbreviations: BRCA1, breast cancer gene 1; TNM, tumor node metastasis; PD-L1, programmed death ligand 1; ITGB1, integrin beta 1; USP51, ubiquitin-specific peptidase 51.

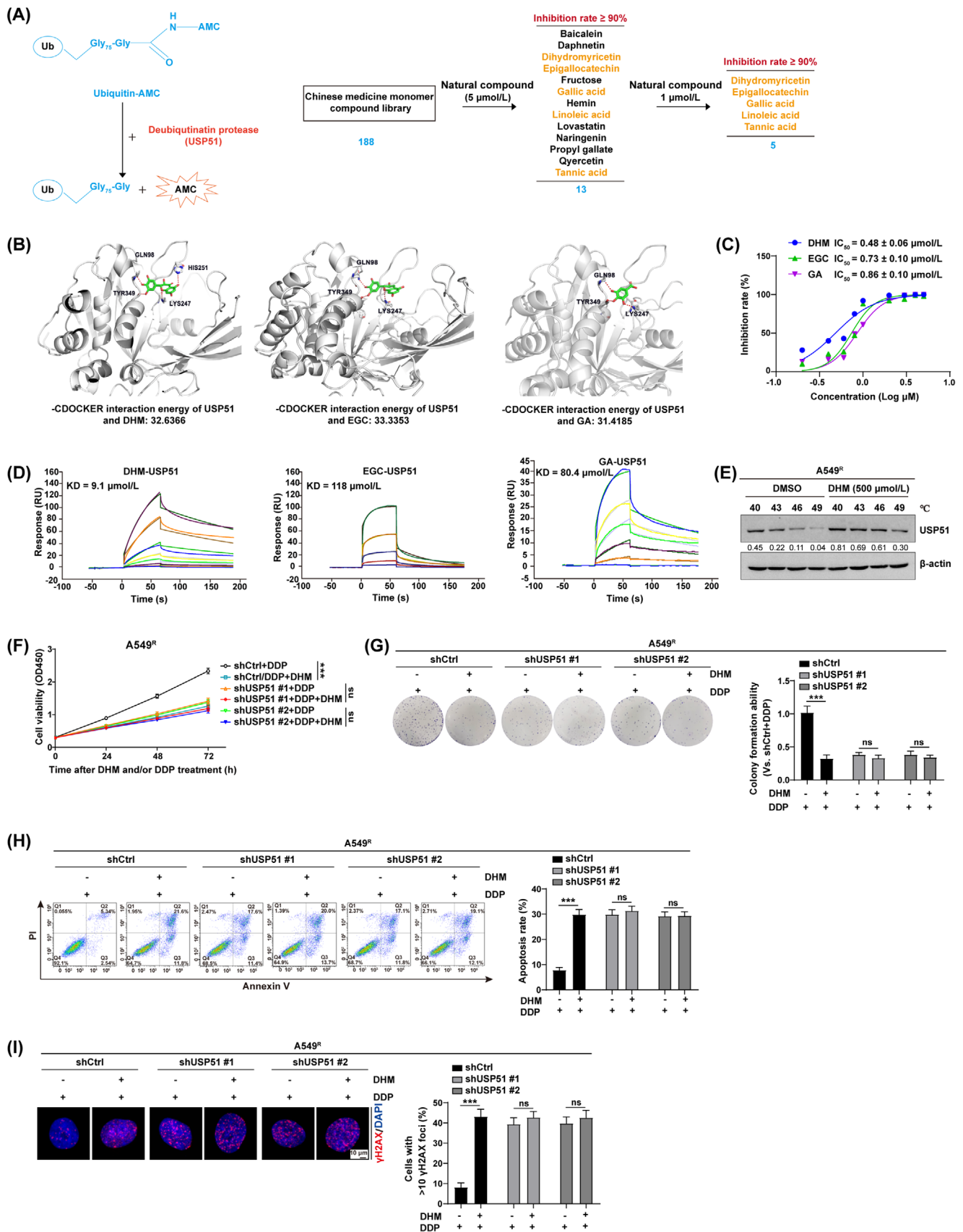


FIGURE 7 DHM acts as a USP51 inhibitor and confers chemosensitization in NSCLC. (A) Screening of USP51 inhibitors was conducted by Ub-AMC assay. (B) The binding affinity between the catalytic domain of USP51 and DHM, EGC and GA was detected by computational molecular dynamic simulation. (C) The inhibitory effect of DHM, EGC and GA on USP51 activity was detected by Ub-AMC assay. (D) The KD values between USP51 and DHM, EGC and GA were measured by SPR binding assay. (E) The binding of USP51 with DHM was detect by

chemotherapeutic treatment in a USP51-dependent manner in NSCLC cells. These experiments were further performed in PC9^R cells and obtained the similar results (Supplementary Figure S23).

3.8 | DHM treatment or ITGB1 neutralization chemosensitized NSCLC

Our study revealed a cell-intrinsic role for USP51/PD-L1/ITGB1 signaling in mediating chemotherapeutic resistance in NSCLC. Therefore, treatment with DHM or anti-ITGB1 might suppress the chemoresistant phenotypes of NSCLC cells and further enhance the efficacy of chemotherapy. To achieve this, A549^R cells were subcutaneously injected into BALB/c nude mice to allow the establishment of primary tumors, then they were treated with DHM, anti-ITGB1 or anti-PD-L1 (avelumab) in the presence of DDP (Figure 8A). We noticed that treatment with DHM or anti-ITGB1 effectively promoted the cell responsiveness to DDP, as evidenced by a reduction in tumor volume (Figure 8B) and weight (Figure 8C) by approximately 75%-80%; however, the combinatorial treatment did not exhibit a synergistic inhibition. Of note, the chemosensitizing efficacy was not shown for anti-PD-L1 treatment, which is consistent with our notion that the cell-intrinsic role of PD-L1 in chemoresistance might not achieve by its interaction with PD-1. The immunohistochemical staining also revealed significant reduction in Ki67 content but increase in cleaved Caspase-3 and γ H2AX expression in tumors with DHM and/or anti-ITGB1 treatment (Figure 8D). No obvious undesirable side effects, namely reduced body weight (Figure 8E) and toxic pathological alterations occurred in the heart, liver, spleen, lung, and kidney (Supplementary Figure S24). Overall, these results implied that disruption of USP51/PD-L1/ITGB1-deployed juxtacrine interaction by treating cancer patients with the USP51 inhibitor (e.g. DHM) or ITGB1 neutralization might inhibit their chemoresistant properties and thus reduce cancer risk.

4 | DISCUSSION

Emerging evidence reported that cancer cell-intrinsic PD-L1 is critical for the development of therapeutic resistance

and is intricately linked to worse NSCLC patient prognosis. Hence, identifying the molecular mechanism that contributes to PD-L1 dysfunction can aid in the design of new and highly efficacious anti-neoplastic treatments. Herein, we demonstrated a cancer cell-intrinsic role of PD-L1 in chemoresistant NSCLC cells, which involves the ITGB1/NF- κ B axis. More importantly, we recognized USP51 as an original deubiquitinase that marked PD-L1 for deubiquitination and stabilization. The specific inhibition of USP51 activity chemosensitized NSCLC cells by promoting PD-L1 protein elimination, which have presented a rationale to target the USP51/PD-L1/ITGB1 axis and prevent its tumor-promoting effects in NSCLC (Figure 8F).

Although it is extensively documented that PD-L1 suppresses anticancer immune response, the cancer cell-intrinsic role of PD-L1 and its association with other oncogenic network garnered much interest [14]. For example, aberrant PD-L1 regulates PI3K/AKT signaling to support tumor survival in NSCLC [40], interacts with phosphorylated STAT3 signaling to facilitate tumor necrosis and progression in breast cancer [41], and modulates tumor glucose metabolism by triggering mTOR signaling in sarcoma [42]. Collectively, our analyses indicated that PD-L1 significantly reduced chemotherapy-mediated killing by stimulating the NF- κ B axis in NSCLC. These observations clearly identified a non-immune checkpoint function of PD-L1 in axis tumor growth, metastasis and therapeutic resistance in multiple cancer types [11, 43]. Mechanistically, we provided additional evidence that PD-L1 mainly functioned through its extracellular domain to interact with ITGB1 as a membrane-bound receptor in chemoresistant NSCLC cells, which supported the notion that aberrant ITGB1 was linked to various chemoresistance-related events, such as defects in tumor growth, apoptosis and genome integrity [44–46]. Importantly, we found that a distinct fragment PD-L1-IgC2, but not PD-L1-IgV, in the PD-L1 extracellular domain was responsible for its direct binding to ITGB1. Thus, PD-L1 blockade using its neutralizing antibody avelumab, which dominantly bound to the PD-L1-IgV domain, might not be sufficient to interrupt PD-L1/ITGB1 interaction and alter cancer cell sensitivity to DDP in NSCLC. Considering that depletion of the PD-L1-IgV domain effectively deprives the interplay between PD-L1 and PD-1 [47, 48], our observations also highlighted that the cancer cell-intrinsic role of PD-L1 in chemoresistance might be independent of its interaction with PD-1.

cellular thermal shift assay in A549^R cells. (F-I) The analyses of cell viability (F), colony formation (G), cell apoptosis (H) and γ H2AX foci formation (I) were examined in shCtrl/A549^R and shPD-L1/A549^R cells following treatment with DHM (60 μ mol/L) and/or DDP (5 μ mol/L). *** $P < 0.001$ and ns represents no obvious difference; (F) was analyzed via two-way ANOVA with Sidak correction for multiple comparisons; (G-I) were assessed via unpaired Student's *t*-test. Abbreviations: Ub-AMC, C-terminal conjugate of ubiquitin with 7-amino-4-methylcoumarin; DHM, dihydromyricetin; EGC, (-)-epigallocatechin; GA, gallic acid; SPR, surface plasmon resonance; DDP, cisplatin; USP51, ubiquitin-specific peptidase 51; γ H2AX, phosphorylated histone H2AX; ANOVA, analysis of variance.

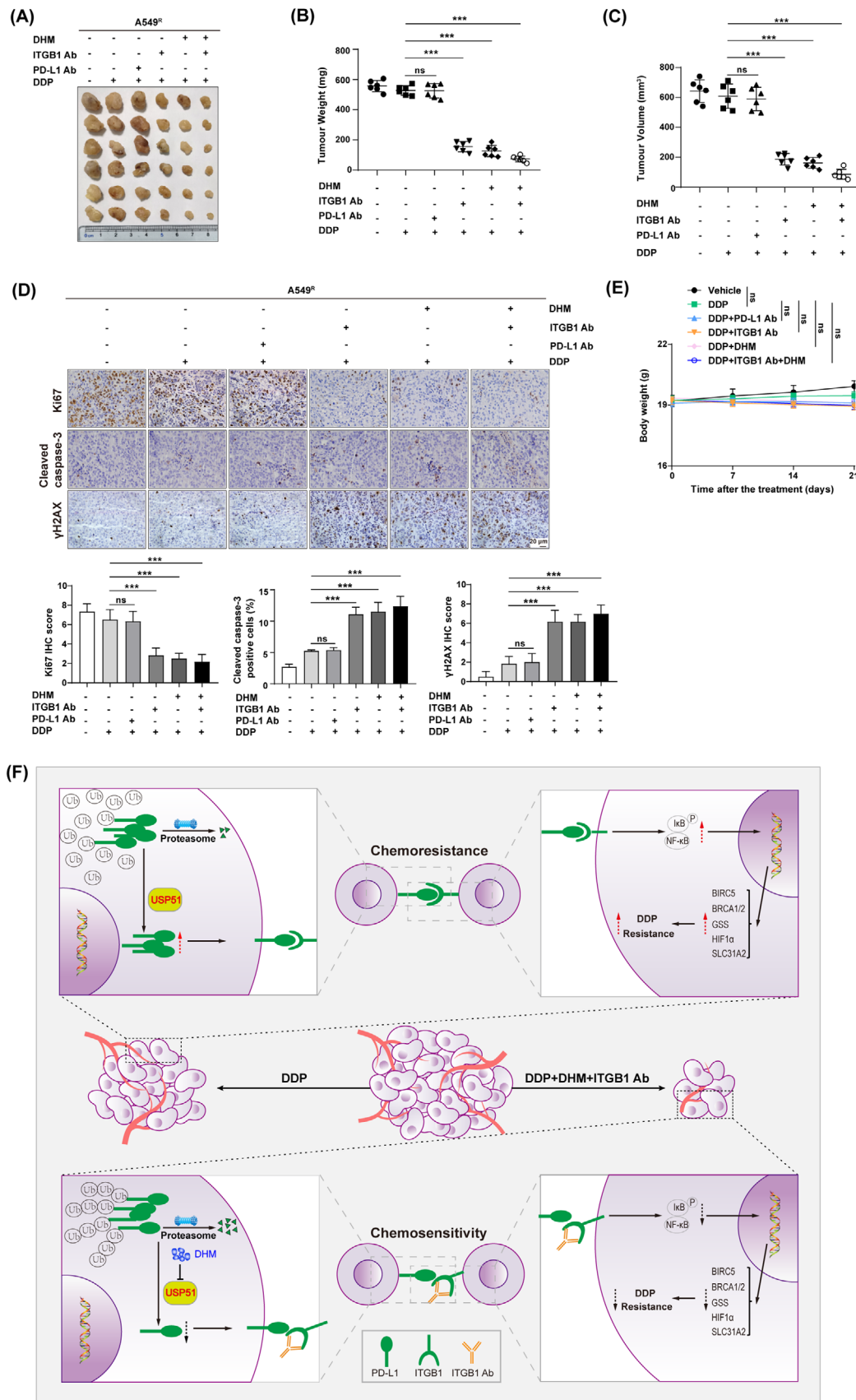


FIGURE 8 DHM treatment or ITGB1 neutralization chemosensitizes NSCLC. (A-E) A549^R cells were subcutaneously administered to NOD-SCID mice following treatment with DHM (100 mg/kg), ITGB1 neutralizing antibody (5 mg/kg) or PD-L1 neutralizing antibody (5 mg/kg) in the presence of DDP. (B-C) The tumor weight (B), tumor volume (C) were shown. (D) The Ki67, cleaved caspase-3 and γH2AX

In line with these, a growing body of evidence have indicated that PD-L1/PD-1 blockage is not completely effective in cancer treatment, as some NSCLC patients remain unresponsive to such treatment [49]. Taken together, these data revealed that a direct correlation between PD-L1 and ITGB1 expression was predominantly present in a subset of advanced NSCLC samples with chemoresistant properties, further detailed investigations on dual blockage of both PD-1 and ITGB1 should be carried out to effectively silence PD-L1 to improve anticancer efficacy.

Several studies have indicated that PD-L1 was highly expressed in numerous solid tumors, particularly NSCLC [50, 51]. Elevated PD-L1 levels are strongly associated with worse clinical outcome in cancer patients [50, 52], which corroborates with the current investigation, which revealed high USP51, PD-L1 and ITGB1 levels in tumors with high tumor grade, advanced TNM stage and poor OS. At the molecular level, mechanisms underlying aberrant PD-L1 expression operate at multiple layers, mainly including genomic alterations, constitutive oncogenic signaling activation, extrinsic factors and epigenetic regulation. For example, *PD-L1* gene amplification on chromosome 9p24.1 has been detected in 5.3% of NSCLC cases [53]. Since the janus kinase 2 (*JAK2*) gene also resides in the 9p24.1 region, increased *JAK2* gene copy number also upregulates PD-L1 levels via the JAK-STAT axis in NSCLC [54]. In addition, a number of cellular stimuli, such as TNF- α [23] and interleukin 17 (IL-17) [55], have been demonstrated to induce PD-L1 expression mainly through interacting with NF- κ B. Several chemotherapeutic agents, such as paclitaxel, can also promote PD-L1 activation via NF- κ B signaling in cancer cells [56]. Here, we extended that study that the cancer cell-intrinsic role of PD-L1 in regulating chemoresistance was predominantly mediated through NF- κ B signaling in NSCLC cells. These data collectively proposed that the constitutive oncogenic NF- κ B signaling activation might create a positive feedback loop to trigger PD-L1 stimulation in malignant progression of human cancers. Indeed, inhibition in NF- κ B activity disrupts this positive feedback loop, which eventually depletes PD-L1 expression and the aggressiveness of NSCLC in vitro and in vivo [35]. On the other hand, both histone acetylation and histone methylation in the *PD-L1* gene promoter region are necessary for abnormal PD-L1 content in solid tumors [57, 58], highlight-

ing the involvement of epigenetic mechanisms in PD-L1 regulation. Considering that histone deacetylase inhibitors exhibited anticancer effect by altering PD-L1 expression in pre-clinical models [59], a combinatorial treatment with histone deacetylase inhibitors and PD-L1 suppression may be a synergistic approach in anticancer therapy.

Besides, the present study expanded on the underlying mechanism by which the PD-L1 content was also regulated posttranslationally in chemoresistant NSCLC cells. We validated that USP51 was an original deubiquitinase that marks the PD-L1 protein for deubiquitination and stabilization. At the molecular level, USP51 directly bound and deubiquitinated PD-L1 at lysine residues K280 and K281. The dominant negative mutants of PD-L1, K280R and/or K281R disrupted the USP51 catalytic activity, but did not alter PD-L1 protein stability. Thus, USP51 was crucial to the induction of chemoresistance through stabilizing PD-L1 protein in NSCLC. In a subset of human NSCLC cell lines and patient samples, USP51 was directly associated with PD-L1 content. Of note, the USP51 and PD-L1 association was strongly evident in NSCLC patients with malignant properties and poor prognosis. More recently, it was reported that ectopic expression of USP51 was able to induce chemoresistant phenotypes, such as DNA damage response, in certain cancer cells [60]. In addition, another deubiquitinase ubiquitin specific peptidase 7 (USP7) had been identified to regulate PD-L1 protein stabilization in gastric cancer [61]. Targeting USP7 with its small molecule inhibitors sensitized cancer cells to T cell-induced destruction by diminishing cell surface PD-L1 content while decreasing its association with PD-1. Hence, small molecule immune checkpoint inhibitors of PD-1/PD-L1 were shown to be highly beneficial in anticancer therapy [12]. These findings also supported our observation that disruption of USP51/PD-L1-deployed juxtacrine interaction with a USP51 inhibitor DHM showed a higher chemotherapeutic efficacy in NSCLC in vitro and in vivo, suggesting that chemo-immunotherapy or a combined treatment of anti-PD-1/PD-L1 with their specific inhibitors could potentially serve a therapeutic role in future anticancer therapies.

The current study had certain limitations. Firstly, the *KRAS* mutations account for approximately 30% of lung adenocarcinomas in Western countries and for 10%-15%

contents were examined by immunohistochemical staining in xenograft tumors. (E) The body weight were shown. (F) A working model indicated the mechanism of USP51/PD-L1/ITGB1 signaling pathway in NSCLC chemoresistance. *** $P < 0.001$ and ns represents no obvious difference; (B-D) were assessed via unpaired Student's *t*-test; (E) was assessed via two-way ANOVA with Sidak correction for multiple comparisons. Abbreviations: DHM, dihydromyricetin; ITGB1 Ab, ITGB1 neutralizing antibody; PD-L1 Ab, PD-L1 neutralizing antibody; DDP, cisplatin; BIRC5, baculoviral IAP repeat containing 5; BRCA1, breast cancer gene 1; BRCA2, breast cancer gene 2; GSS, glutathione synthetase; HIF1 α , hypoxia inducible factor 1 alpha; SLC31A2, solute carrier family 31 member 2; PD-L1, programmed death ligand 1; ITGB1, integrin beta 1; USP51, ubiquitin-specific peptidase 51; γ H2AX, phosphorylated histone H2AX; ANOVA, analysis of variance.

of cases in Asia [62]. For example, the *KRAS*^{G12C} mutation is highly prevalent in patients suffering from lung adenocarcinoma (13% of total lung adenocarcinoma) and account for approximately 50% of all *KRAS* mutant cases [63]. The present study was lack of NSCLC cell lines with the *KRAS*^{G12C} mutation, such as H23 and H358 cells [64]. Thus, further studies are required to obtain a more comprehensive understanding. Secondly, due to the low water solubility and chemical stability of DHM, additional research should be carried out to investigate the characteristic and mechanism for inclusion of DHM and evaluate the effects of complexation on antitumor activities of DHM by targeting USP51.

5 | CONCLUSIONS

Herein, we proposed a novel signaling network involving the USP51/PD-L1/ITGB1 axis that modulates NSCLC chemoresistance, which supplements the immune-free and cancer cell-intrinsic roles of PD-L1. Given that deubiquitinases are susceptible to pharmacology-mediated suppression, targeting USP51 using small molecule inhibitor (e.g., DHM) to reduce PD-L1 stability in conjunction with anti-PD-1 and/or anti-ITGB1 treatment represents a new therapeutic strategy that could efficiently impair PD-L1 and thus limit local tumor growth and aggressive progression in NSCLC.

DECLARATIONS

AUTHOR CONTRIBUTIONS

Conception and design: JL, XX, GY and SY; Development of methodology: JL, XX, YO, LC, MG, HW, GY and SY; Analysis and interpretation of data (for example, statistical analysis, biostatistics, computational analysis): JL, XX, CQ, ZW, YL, QS, PS, YS, GY and SY; Writing, review of the manuscript: JL, XX, PS, YS, GY and SY.

ACKNOWLEDGMENTS

This work was supported by grants from the International Science and Technology Cooperation Project of China (No. 2022YFE0133300) and National Natural Science Foundation of China (No. 82172801 and No. 81972454).

CONFLICT OF INTEREST STATEMENT

The authors declare that they have no conflict of interest.

ETHICS APPROVAL AND CONSENT TO PARTICIPATE

This study was approved by the Ethics Committee of Nankai University (NKUIRB2021010). The tissue samples were obtained with written informed consent from each patient. All of the experimental procedures involv-

ing animals were performed in accordance with a protocol that was approved by the Ethics Committee for Animal Use at the Medical College of Nankai University (2021-SYDWLL-000040).

CONSENT FOR PUBLICATION

Not applicable.

DATA AVAILABILITY STATEMENT

The data that support the findings of this study are available from the corresponding author upon reasonable request.

ORCID

Shuang Yang  <https://orcid.org/0000-0002-4779-8553>

REFERENCES

1. Siegel RL, Miller KD, Fuchs HE, Jemal A. Cancer Statistics, 2021. *CA Cancer J Clin*. 2021;71(1):7–33.
2. Srivastava S, Mohanty A, Nam A, Singhal S, Salgia R. Chemokines and NSCLC: Emerging role in prognosis, heterogeneity, and therapeutics. *Semin Cancer Biol*. 2022;86(Pt 2):233–46.
3. Wang M, Herbst RS, Boshoff C. Toward personalized treatment approaches for non-small-cell lung cancer. *Nat Med*. 2021;27(8):1345–56.
4. Terlizzi M, Colarusso C, Pinto A, Sorrentino R. Drug resistance in non-small cell lung Cancer (NSCLC): Impact of genetic and non-genetic alterations on therapeutic regimen and responsiveness. *Pharmacol Ther*. 2019;202:140–8.
5. Kornepati AVR, Vadlamudi RK, Curiel TJ. Programmed death ligand 1 signals in cancer cells. *Nat Rev Cancer*. 2022;22(3):174–89.
6. Chang JY, Verma V, Welsh JW, Formenti SC. Radiotherapy plus immune checkpoint blockade in PD(L)-I-resistant metastatic NSCLC. *Lancet Oncol*. 2022;23(4):e156.
7. Lv H, Lv G, Chen C, Zong Q, Jiang G, Ye D, et al. NAD(+) Metabolism Maintains Inducible PD-L1 Expression to Drive Tumor Immune Evasion. *Cell Metab*. 2021;33(1):110–27.e5.
8. Zhang X, Lao M, Xu J, Duan Y, Yang H, Li M, et al. Combination cancer immunotherapy targeting TNFR2 and PD-1/PD-L1 signaling reduces immunosuppressive effects in the microenvironment of pancreatic tumors. *J Immunother Cancer*. 2022;10(3):e003982.
9. Sharma P, Hu-Lieskovan S, Wargo JA, Ribas A. Primary, Adaptive, and Acquired Resistance to Cancer Immunotherapy. *Cell*. 2017;168(4):707–23.
10. Tu X, Qin B, Zhang Y, Zhang C, Kahila M, Nowsheen S, et al. PD-L1 (B7-H1) Competes with the RNA Exosome to Regulate the DNA Damage Response and Can Be Targeted to Sensitize to Radiation or Chemotherapy. *Mol Cell*. 2019;74(6):1215–26.e4.
11. Cao D, Qi Z, Pang Y, Li H, Xie H, Wu J, et al. Retinoic Acid-Related Orphan Receptor C Regulates Proliferation, Glycolysis, and Chemoresistance via the PD-L1/ITGB6/STAT3 Signaling Axis in Bladder Cancer. *Cancer Res*. 2019;79(10):2604–18.

12. Zhang J, Bu X, Wang H, Zhu Y, Geng Y, Nihira NT, et al. Cyclin D-CDK4 kinase destabilizes PD-L1 via cullin 3-SPOP to control cancer immune surveillance. *Nature*. 2018;553(7686):91–5.
13. Wang S, Li J, Xie J, Liu F, Duan Y, Wu Y, et al. Programmed death ligand 1 promotes lymph node metastasis and glucose metabolism in cervical cancer by activating integrin β 4/SNAI1/SIRT3 signaling pathway. *Oncogene*. 2018;37(30):4164–80.
14. Cha JH, Chan LC, Li CW, Hsu JL, Hung MC. Mechanisms Controlling PD-L1 Expression in Cancer. *Mol Cell*. 2019;76(3):359–70.
15. Masuda J, Ozaki Y, Hara F, Kitano S, Takano T. Pembrolizumab plus chemotherapy in triple-negative breast cancer. *Lancet*. 2021;398(10294):24.
16. Sun L, Patai Á V, Hogenson TL, Fernandez-Zapico ME, Qin B, Sinicrope FA. Irreversible JNK blockade overcomes PD-L1-mediated resistance to chemotherapy in colorectal cancer. *Oncogene*. 2021;40(32):5105–15.
17. Zhang X, Zeng Y, Qu Q, Zhu J, Liu Z, Ning W, et al. PD-L1 induced by IFN- γ from tumor-associated macrophages via the JAK/STAT3 and PI3K/AKT signaling pathways promoted progression of lung cancer. *Int J Clin Oncol*. 2017;22(6):1026–33.
18. Gao Y, Yang J, Cai Y, Fu S, Zhang N, Fu X, et al. IFN- γ -mediated inhibition of lung cancer correlates with PD-L1 expression and is regulated by PI3K-AKT signaling. *Int J Cancer*. 2018;143(4):931–43.
19. Hu ZY, Huang WY, Zhang L, Huang B, Chen SC, Li XL. Expression of AKT and p-AKT protein in lung adenocarcinoma and its correlation with PD-L1 protein and prognosis. *Ann Transl Med*. 2020;8(18):1172.
20. Tang H, Liu Y, Wang C, Zheng H, Chen Y, Liu W, et al. Inhibition of COX-2 and EGFR by Melafolone Improves Anti-PD-1 Therapy through Vascular Normalization and PD-L1 Downregulation in Lung Cancer. *J Pharmacol Exp Ther*. 2019;368(3):401–13.
21. Tang Z, Pilié PG, Geng C, Manyam GC, Yang G, Park S, et al. ATR Inhibition Induces CDK1-SPOP Signaling and Enhances Anti-PD-L1 Cytotoxicity in Prostate Cancer. *Clin Cancer Res*. 2021;27(17):4898–909.
22. Li CW, Lim SO, Xia W, Lee HH, Chan LC, Kuo CW, et al. Glycosylation and stabilization of programmed death ligand-1 suppresses T-cell activity. *Nat Commun*. 2016;7:12632.
23. Lim SO, Li CW, Xia W, Cha JH, Chan LC, Wu Y, et al. Deubiquitination and Stabilization of PD-L1 by CSN5. *Cancer Cell*. 2016;30(6):925–39.
24. Zhang Z, Li J, Ou Y, Yang G, Deng K, Wang Q, et al. CDK4/6 inhibition blocks cancer metastasis through a USP51-ZEB1-dependent deubiquitination mechanism. *Signal Transduct Target Ther*. 2020;5(1):25.
25. Chang A, Liu L, Ashby JM, Wu D, Chen Y, O'Neill SS, et al. Recruitment of KMT2C/MLL3 to DNA Damage Sites Mediates DNA Damage Responses and Regulates PARP Inhibitor Sensitivity in Cancer. *Cancer Res*. 2021;81(12):3358–73.
26. Liu K, Tan S, Chai Y, Chen D, Song H, Zhang CW, et al. Structural basis of anti-PD-L1 monoclonal antibody avelumab for tumor therapy. *Cell Res*. 2017;27(1):151–3.
27. Phatak P, Byrnes KA, Mansour D, Liu L, Cao S, Li R, et al. Overexpression of miR-214-3p in esophageal squamous cancer cells enhances sensitivity to cisplatin by targeting survivin directly and indirectly through CUG-BP1. *Oncogene*. 2016;35(16):2087–97.
28. Wang H, Huang Y, Shi J, Zhi Y, Yuan F, Yu J, et al. XPC deficiency leads to centrosome amplification by inhibiting BRCA1 expression upon cisplatin-mediated DNA damage in human bladder cancer. *Cancer Lett*. 2019;444:136–46.
29. Cong K, Peng M, Kousholt AN, Lee WTC, Lee S, Nayak S, et al. Replication gaps are a key determinant of PARP inhibitor synthetic lethality with BRCA deficiency. *Mol Cell*. 2021;81(15):3128–44.e7.
30. Stok C, Kok YP, van den Tempel N, van Vugt M. Shaping the BRCAness mutational landscape by alternative double-strand break repair, replication stress and mitotic aberrancies. *Nucleic Acids Res*. 2021;49(8):4239–57.
31. Sun H, Zhou R, Zheng Y, Wen Z, Zhang D, Zeng D, et al. CRIP1 cooperates with BRCA2 to drive the nuclear enrichment of RAD51 and to facilitate homologous repair upon DNA damage induced by chemotherapy. *Oncogene*. 2021;40(34):5342–55.
32. Zhang J, Zhao B, Chen S, Wang Y, Zhang Y, Wang Y, et al. Near-Infrared Light Irradiation Induced Mild Hyperthermia Enhances Glutathione Depletion and DNA Interstrand Cross-Link Formation for Efficient Chemotherapy. *ACS Nano*. 2020;14(11):14831–45.
33. Li Z, Zhou W, Zhang Y, Sun W, Yung MMH, Sun J, et al. ERK Regulates HIF1 α -Mediated Platinum Resistance by Directly Targeting PHD2 in Ovarian Cancer. *Clin Cancer Res*. 2019;25(19):5947–60.
34. Blair BG, Larson CA, Safaei R, Howell SB. Copper transporter 2 regulates the cellular accumulation and cytotoxicity of Cisplatin and Carboplatin. *Clin Cancer Res*. 2009;15(13):4312–21.
35. Antonangeli F, Natalini A, Garassino MC, Sica A, Santoni A, Di Rosa F. Regulation of PD-L1 Expression by NF- κ B in Cancer. *Front Immunol*. 2020;11:584626.
36. Jirawatnotai S, Hu Y, Michowski W, Elias JE, Becks L, Bienvenu F, et al. A function for cyclin D1 in DNA repair uncovered by protein interactome analyses in human cancers. *Nature*. 2011;474(7350):230–4.
37. Casimiro MC, Di Sante G, Ju X, Li Z, Chen K, Crosariol M, et al. Cyclin D1 Promotes Androgen-Dependent DNA Damage Repair in Prostate Cancer Cells. *Cancer Res*. 2016;76(2):329–38.
38. Álvarez-Quilón A, Wojtaszek JL, Mathieu MC, Patel T, Appel CD, Hustedt N, et al. Endogenous DNA 3' Blocks Are Vulnerabilities for BRCA1 and BRCA2 Deficiency and Are Reversed by the APE2 Nuclease. *Mol Cell*. 2020;78(6):1152–65.e8.
39. Kraiss JJ, Wang Y, Patel P, Basu J, Bernhardt AJ, Johnson N. RNF168-mediated localization of BARD1 recruits the BRCA1-PALB2 complex to DNA damage. *Nat Commun*. 2021;12(1):5016.
40. Yu W, Hua Y, Qiu H, Hao J, Zou K, Li Z, et al. PD-L1 promotes tumor growth and progression by activating WIP and β -catenin signaling pathways and predicts poor prognosis in lung cancer. *Cell Death Dis*. 2020;11(7):506.
41. Hou J, Zhao R, Xia W, Chang CW, You Y, Hsu JM, et al. PD-L1-mediated gasdermin C expression switches apoptosis to pyroptosis in cancer cells and facilitates tumour necrosis. *Nat Cell Biol*. 2020;22(10):1264–75.
42. Chang CH, Qiu J, O'Sullivan D, Buck MD, Noguchi T, Curtis JD, et al. Metabolic Competition in the Tumor Microenvironment Is a Driver of Cancer Progression. *Cell*. 2015;162(6):1229–41.
43. Sun L, Huang C, Zhu M, Guo S, Gao Q, Wang Q, et al. Gastric cancer mesenchymal stem cells regulate PD-L1-CTCF

- enhancing cancer stem cell-like properties and tumorigenesis. *Theranostics*. 2020;10(26):11950–62.
44. Huang L, Hu C, Chao H, Wang R, Lu H, Li H, et al. miR-29c regulates resistance to paclitaxel in nasopharyngeal cancer by targeting ITGB1. *Exp Cell Res*. 2019;378(1):1–10.
 45. Marusak C, Thakur V, Li Y, Freitas JT, Zmina PM, Thakur VS, et al. Targeting Extracellular Matrix Remodeling Restores BRAF Inhibitor Sensitivity in BRAFi-resistant Melanoma. *Clin Cancer Res*. 2020;26(22):6039–50.
 46. Kinehara Y, Nagatomo I, Koyama S, Ito D, Nojima S, Kurebayashi R, et al. Semaphorin 7A promotes EGFR-TKI resistance in EGFR mutant lung adenocarcinoma cells. *JCI Insight*. 2018;3(24):e123093.
 47. Vandeveer AJ, Fallon JK, Tighe R, Sabzevari H, Schlom J, Greiner JW. Systemic Immunotherapy of Non-Muscle Invasive Mouse Bladder Cancer with Avelumab, an Anti-PD-L1 Immune Checkpoint Inhibitor. *Cancer Immunol Res*. 2016;4(5):452–62.
 48. Grenga I, Donahue RN, Lepone LM, Richards J, Schlom J. A fully human IgG1 anti-PD-L1 MAb in an in vitro assay enhances antigen-specific T-cell responses. *Clin Transl Immunology*. 2016;5(5):e83.
 49. Lei Q, Wang D, Sun K, Wang L, Zhang Y. Resistance Mechanisms of Anti-PD1/PDL1 Therapy in Solid Tumors. *Front Cell Dev Biol*. 2020;8:672.
 50. Brody R, Zhang Y, Ballas M, Siddiqui MK, Gupta P, Barker C, et al. PD-L1 expression in advanced NSCLC: Insights into risk stratification and treatment selection from a systematic literature review. *Lung Cancer*. 2017;112:200–15.
 51. Wang H, Shan Q, Guo J, Han X, Zhao C, Li H, et al. PDL1 high expression without TP53, KEAP1 and EPHA5 mutations could better predict survival for patients with NSCLC receiving atezolizumab. *Lung Cancer*. 2021;151:76–83.
 52. Aguilar EJ, Ricciuti B, Gainor JF, Kehl KL, Kravets S, Dahlberg S, et al. Outcomes to first-line pembrolizumab in patients with non-small-cell lung cancer and very high PD-L1 expression. *Ann Oncol*. 2019;30(10):1653–9.
 53. Green MR, Monti S, Rodig SJ, Juszczynski P, Currie T, O'Donnell E, et al. Integrative analysis reveals selective 9p24.1 amplification, increased PD-1 ligand expression, and further induction via JAK2 in nodular sclerosing Hodgkin lymphoma and primary mediastinal large B-cell lymphoma. *Blood*. 2010;116(17):3268–77.
 54. Clavé S, Pijuan L, Casadevall D, Taus Á, Gimeno J, Hernández-Llodrà S, et al. CD274 (PDL1) and JAK2 genomic amplifications in pulmonary squamous-cell and adenocarcinoma patients. *Histopathology*. 2018;72(2):259–69.
 55. Wang X, Yang L, Huang F, Zhang Q, Liu S, Ma L, et al. Inflammatory cytokines IL-17 and TNF- α up-regulate PD-L1 expression in human prostate and colon cancer cells. *Immunol Lett*. 2017;184:7–14.
 56. Peng J, Hamanishi J, Matsumura N, Abiko K, Murat K, Baba T, et al. Chemotherapy Induces Programmed Cell Death-Ligand 1 Overexpression via the Nuclear Factor- κ B to Foster an Immunosuppressive Tumor Microenvironment in Ovarian Cancer. *Cancer Res*. 2015;75(23):5034–45.
 57. Wang H, Fu C, Du J, Wang H, He R, Yin X, et al. Enhanced histone H3 acetylation of the PD-L1 promoter via the COP1/c-Jun/HDAC3 axis is required for PD-L1 expression in drug-resistant cancer cells. *J Exp Clin Cancer Res*. 2020;39(1):29.
 58. Lv D, Xing C, Cao L, Zhuo Y, Wu T, Gao N. PD-L1 gene promoter methylation represents a potential diagnostic marker in advanced gastric cancer. *Oncol Lett*. 2020;19(2):1223–34.
 59. Hu X, Lin Z, Wang Z, Zhou Q. Emerging role of PD-L1 modification in cancer immunotherapy. *Am J Cancer Res*. 2021;11(8):3832–40.
 60. Wang Z, Zhang H, Liu J, Cheruiyot A, Lee JH, Ordog T, et al. USP51 deubiquitylates H2AK13,15ub and regulates DNA damage response. *Genes Dev*. 2016;30(8):946–59.
 61. Wang Z, Kang W, Li O, Qi F, Wang J, You Y, et al. Abrogation of USP7 is an alternative strategy to downregulate PD-L1 and sensitize gastric cancer cells to T cells killing. *Acta Pharm Sin B*. 2021;11(3):694–707.
 62. Dearden S, Stevens J, Wu YL, Blowers D. Mutation incidence and coincidence in non small-cell lung cancer: meta-analyses by ethnicity and histology (mutMap). *Ann Oncol*. 2013;24(9):2371–6.
 63. Bar-Sagi D, Knelson EH, Sequist LV. A bright future for KRAS inhibitors. *Nat Cancer*. 2020;1(1):25–7.
 64. Suzuki S, Yonesaka K, Teramura T, Takehara T, Kato R, Sakai H, et al. KRAS Inhibitor Resistance in MET-Amplified KRAS (G12C) Non-Small Cell Lung Cancer Induced By RAS- and Non-RAS-Mediated Cell Signaling Mechanisms. *Clin Cancer Res*. 2021;27(20):5697–707.

SUPPORTING INFORMATION

Additional supporting information can be found online in the Supporting Information section at the end of this article.

How to cite this article: Li J, Xiao X, Ou Y, Cao L, Guo M, Qi C, et al. USP51/PD-L1/ITGB1-deployed juxtacrine interaction plays a cell-intrinsic role in promoting chemoresistant phenotypes in non-small cell lung cancer. *Cancer Commun*. 2023;1–23. <https://doi.org/10.1002/cac2.12460>